CHAPTER 4

RESULTS AND DISCUSSIONS CERAMIC IN THE OF xBa($Mg_{1/3}Nb_{2/3}$)O_3-(1-x)$BaTiO_3$ SYSTEM

This chapter presents the results of the investigation on the phase evolution, microstructure and dielectric properties of BT based capacitor doped with BMN with different 2 processing (P1 and P2). The results are identified and discussed.

4.1 Particle Size Analysis of Powders

The particle size measurement was analyzed due to identify the size of starting powders before sintering according to the sample composition and particle size shown in TABLE 4.1. From the results, the particle size of powders from P1 processing showed smaller than from P2 processing. It is expected, however, that the agglomerate between the base compound and additives will possibly yield high the average particle size as be seen in Figure 4.1(a), (b).

TABLE 4.1 Particle size of xBa($Mg_{1/3}Nb_{2/3}$)O_3-(1-x)$BaTiO_3$ by P1 and P2 processing

Composition x	Mean Diameter (μm)	
	P1 Processing	P2 Processing
$BaTiO_3$	1.23	-
0.01	0.92	1.20
0.02	1.56	2.13
0.03	1.26	0.94
0.04	1.30	1.67
0.05	1.02	3.15
0.06	1.06	4.39
0.07	0.84	3.95
Ba($Mg_{1/3}Nb_{2/3}$)O_3	0.64	-

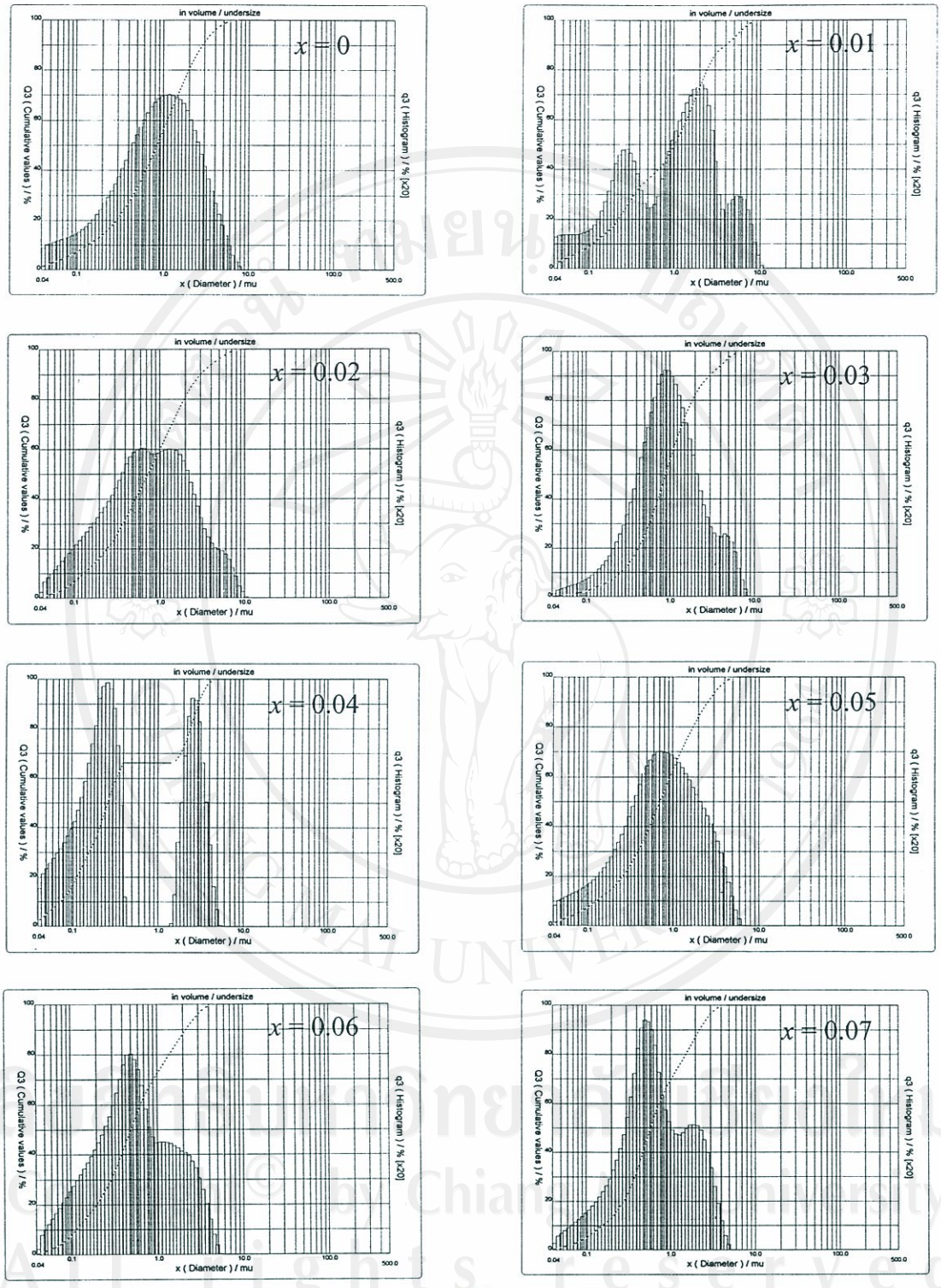

(a)

Figure 4.1(a) The particle size distribution of xBa($Mg_{1/3}Nb_{2/3}$)O_3-(1-x)$BaTiO_3$ powder with as function of x prepared by P1 processing.

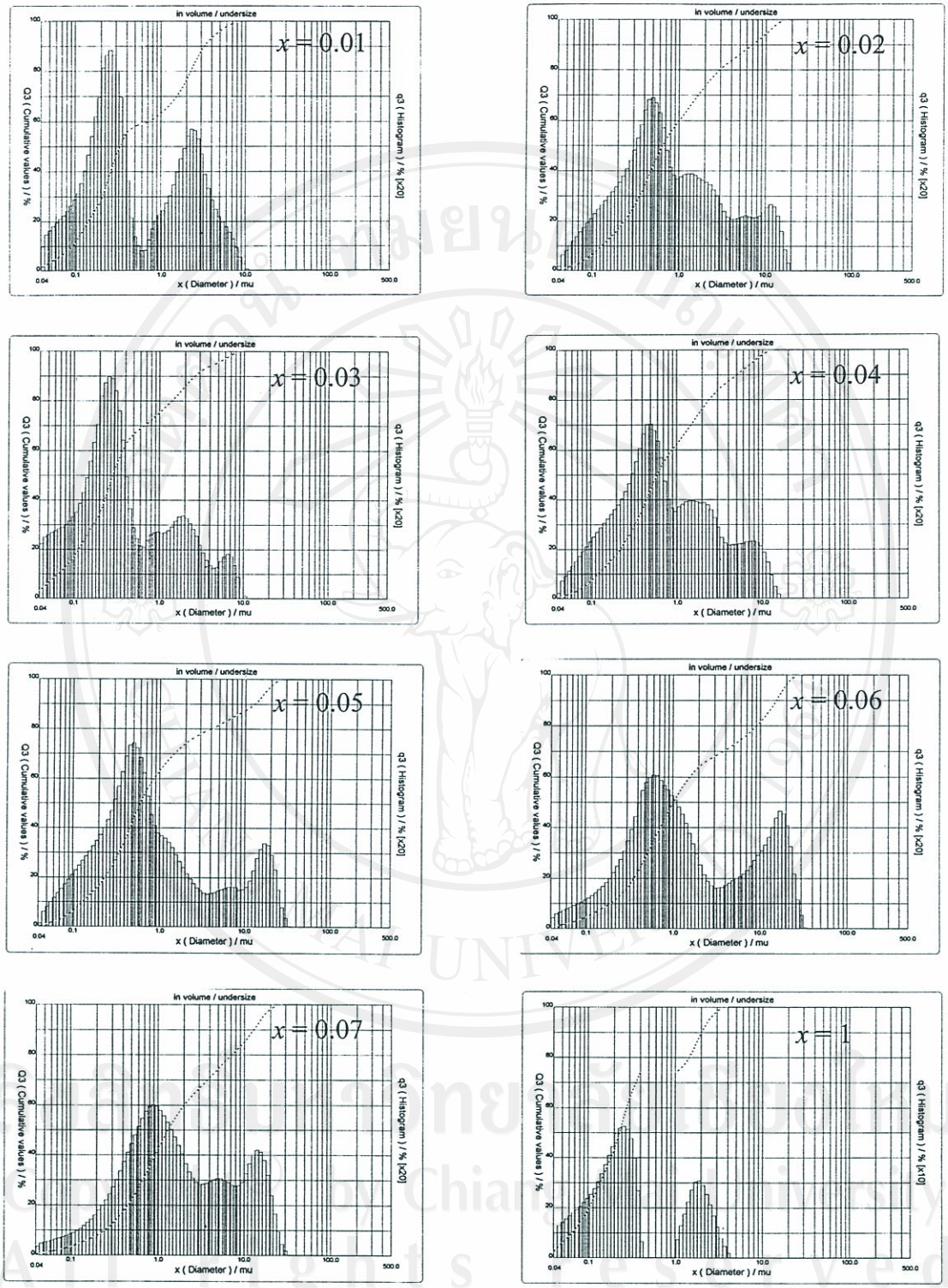

(b)

Figure 4.1(b) The particle size distribution of $x\text{Ba}(\text{Mg}_{1/3}\text{Nb}_{2/3})\text{O}_3\text{-}(1\text{-}x)\text{BaTiO}_3$ powder with as function of x prepared by P2 processing.

4.2 Phase Identification by XRD

The BMN-substituted BT, i.e. $x\text{Ba}(\text{Mg}_{1/3}\text{Nb}_{2/3})\text{O}_3\text{-}(1\text{-}x)\text{BaTiO}_3$ powder with x = 0-0.07 were identified the phase formation by XRD technique. The perovskite phase formation and crystal structure of powders were detected at room temperature as a function of x. It can be shown in Figure 4.2(a), (b). The analysis was carried out based on the Joint Committee on Powder Diffraction Standard (JCPDS). From the result, it was found that all the lines could be attributed to BT phase as cubic which could be matched with JCPDS file No. 79-2263 [53] and unidentified peak at d = 3.03 were found in both processing (P1 and P2) with x = 0. No evidence of residual precursors was detected by this technique for powders from P1 processing (where x = 0.01-0.07) as can be shown in Figure 4.2(a). However, the XRD patterns of powders from P2 processing showed the extra-peaks of second phase with $x \geq 0.03$ but more clearly at x = 0.07. From the Figure 4.2(b), the second phase was contributed as BMN precursor which could be matched with JCPDS file No. 17-0173 [54]. The broadening peaks were found due to cause by chemical inhomogeneities in the powder mixture, and in complete solid solution during calcinations. The localized variations in solid solution composition of Ti ion and Nb and/or Mg ion give a variety of slightly different lattice parameters, and broadened XRD peaks.

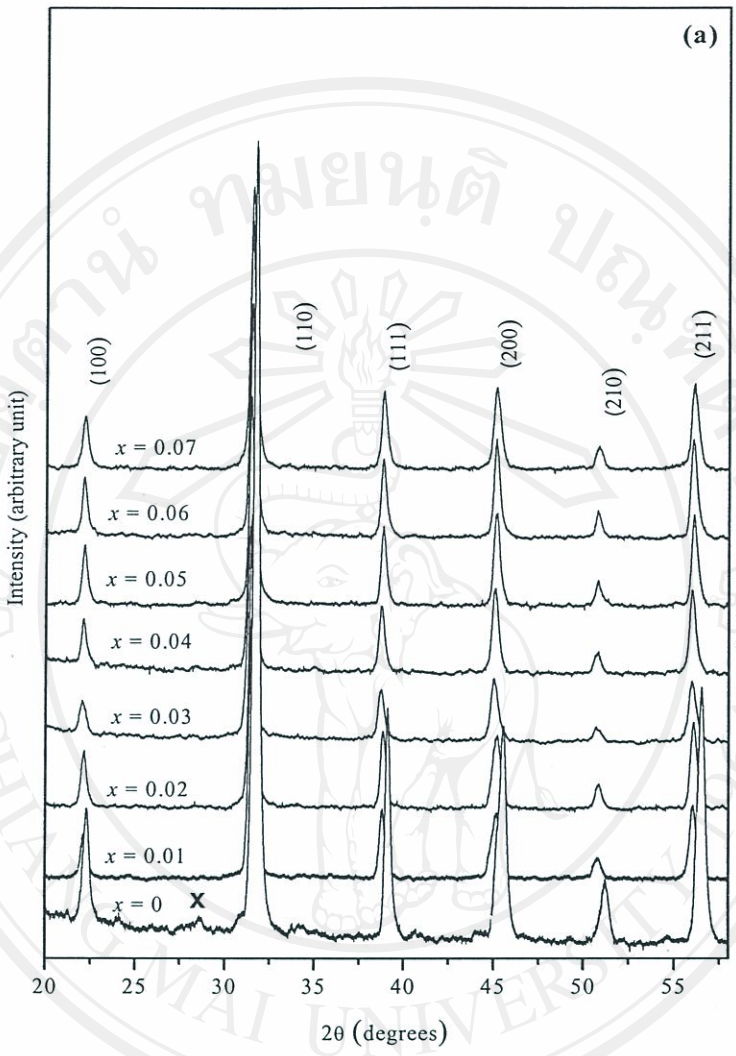

Figure 4.2(a) Shows the XRD patterns of calcined powders of xBa($Mg_{1/3}Nb_{2/3}$)O_3 -(1-x)$BaTiO_3$ prepared by (a) P1 processing (b) P2 processing ; x indicating unidentified peak.

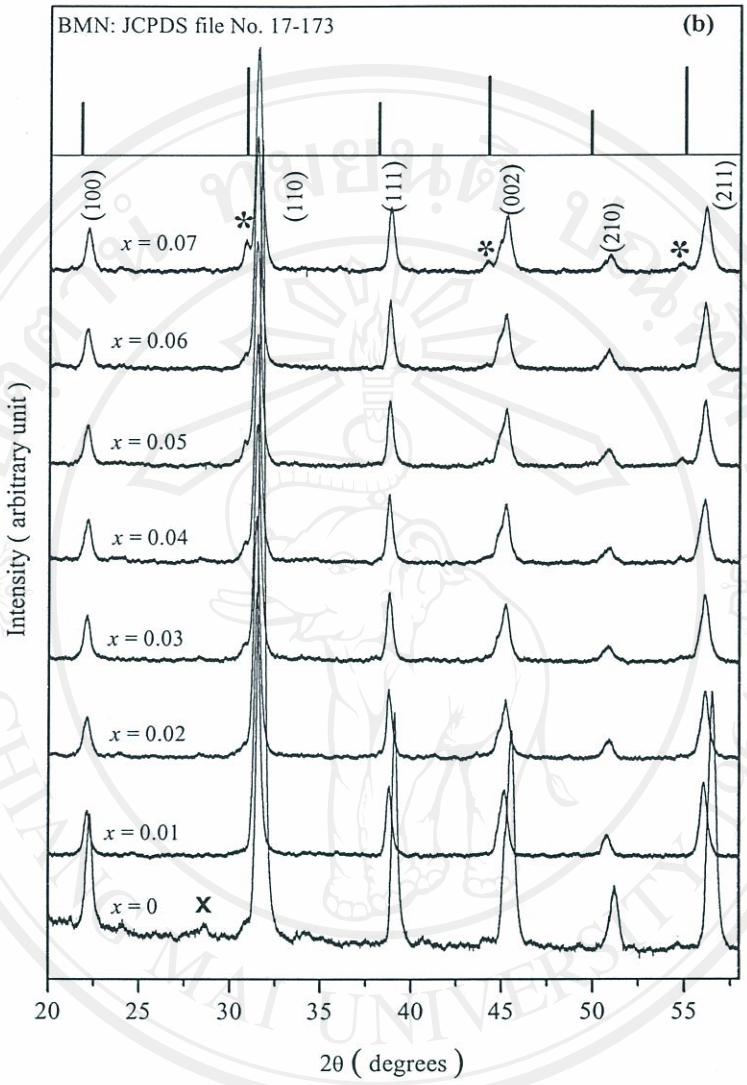

Figure 4.2(b) Shows the XRD patterns of calcined powders of xBa($Mg_{1/3}Nb_{2/3}$)O_3 - (1-x)$BaTiO_3$ prepared by (a) P1 processing (b) P2 processing; x indicating unidentified peak and * indicating as BMN.

In case of ceramic, the effect of processing and additives, BMN on ceramic with using P1 and P2 processing preparation was investigated. Phase evolution of ceramic with various amount of BMN was compared by XRD technique. Phase formation and crystal structure of ceramics were detected at room temperature as a function of x as shown in Figure 4.3-4.6.

The XRD patterns showed the shape peaks indicated the good crystalline which could be attributed to BT as main phase for both processing method. The results indicated that for the same composition, different processing method may develop the perovskite structure with different symmetry. The slightly different of phase evolution was found in XRD pattern compared with both processing. Figure 4.3 (a) showed the phase evolution of sintered ceramic (P1 processing) with as a function of x. From the data, the coexistence of cubic phase [53] and tetragonal phase [55] at room temperature were found with low concentration of BMN between 0-0.04. At x = 0.05, its crystal structure became cubic due to the X-ray profile was no splitting of (200) and (002) peaks. Moreover, the phase transformation to be pseudocubic as rhombohedral phase [22, 56] was found at highest amount of BMN in this study as x = 0.07. The cubic–tetragonal transformation phenomenon for BMN doped BT ceramic was quite agreed with Weill *et al.* [42,43] who found the same result with though employing chemical route in preparation. It is widely accepted that the deformed cubic (pseudocubic) phase exists at room temperature [57-59]. The lattice distortion that can occurs within BT doped at room temperature is believed to be due to a replacement of Mg and Nb cation which have the different ionic radius. As can be seen, these changes were accompanied by a decrease in the c lattice parameter, and corresponding increased lattice strain with accompanying

development of the pseudocubic phase. This result is quite agreed with Henning and Armstrong [58-59] who found pseudocubic phase in Zr doped BT. The solid solubility of Mg and Nb cation in the BT lattice is expected to be limited. Especially Mg ion, it widely know that to be inert/low reactivity chemical reagent. Figure 4.3(b) showed the zoom in the XRD patterns of samples with x = 0.01, 0.04 and 0.07 from P1 processing to identify the small extra peaks at low intensity. The extra peaks were compared with standard XRD files suggested these present the second phase as $Ba_6Ti_{17}O_{40}$ [60] at low concentration of additives and no evident the Mg second phase in P1 system. It is possibly due to Mg and Nb ions can diffuse easier than BMN or Mg second phase amount has a lower level than that of the XRD detection limit. This result has been reported by Tkach [14] who found that BT system exceed 10 percent, showing for higher Mg concentrations the appearance of a MgO second phase. Consequently the incorporation of Mg ions into the B sublattice of BT is favorable and a higher solid solubility limit was achieved.

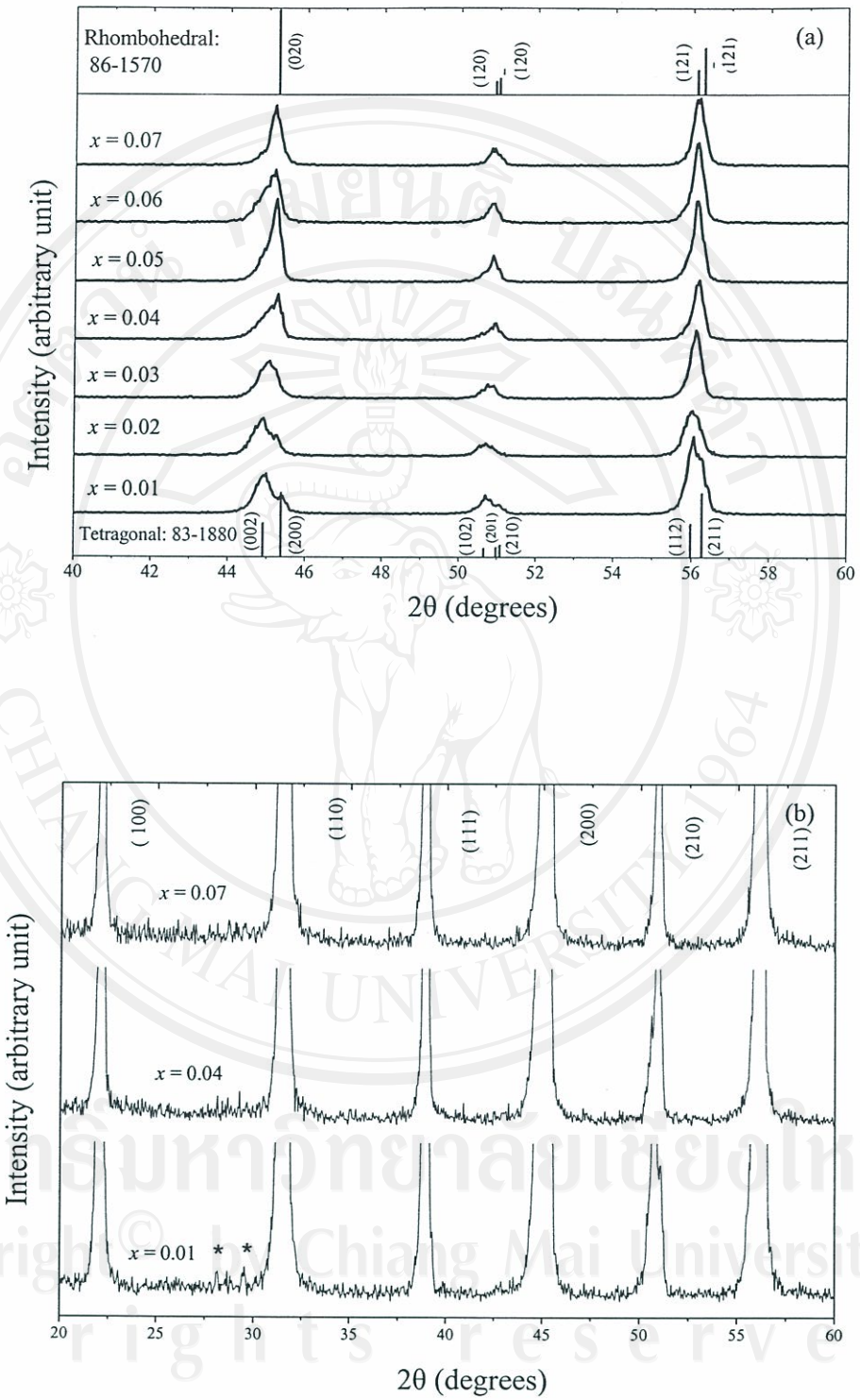

Figure 4.3 X-ray diffractions of samples sintered at 1450°C from P1 processing showing; (a) phase formation as a function of x and (b) second phase formation; * indicating $Ba_6Ti_{17}O_{40}$.

In case of P2 sintered samples, all the peaks showed the good crystalline as well but unclear phase transformation was found in this system. The data confirmed the tetragonal splitting at high angles with $x = 0.02$ of additives of P1 and P2 ceramic sample was shown in Figure 4.4, exhibited that the clearer tetragonal splitting was found in P1 sample than that P2. This indicated the slightly higher order of tetragonality of P1 samples cause by different starting precursor. At low concentration of $x = 0.01$–0.04 of BMN, the X-ray profile was characterized by two broad peaks with no distinct splitting. And at 0.05–0.06, the X-ray pattern showed the tetragonal splitting of (200) and (002) peaks were merged became one that indicated the cubic phase transformation. So, the estimation of cubic–tetragonal transformation was expected between of $x = 0.05$-0.06 of added samples by P2 processing, it can be seen in Figure 4.5 (a). The solid solubility of BMN as precursor in the BT lattice is expected to be limited. The XRD results obtained in this work confirm the expectation. For the P2 system indicated a very weak BMN solubility in BT lattice. Figure 4.5(b) showed the zoom in the XRD patterns of samples with $x = 0.01$, 0.04 and 0.07 from P2 processing to identify the small extra peaks at low intensity. Comparison made with standard XRD files at $x = 0.04$ of BMN added ceramic sample suggested present the maximum of complex secondary phase mixture of $Ba_6Ti_{17}O_{40}$, $Ba_4MgTi_{11}O_{27}$ [61] and $Ba(Mg_{1/3}Nb_{2/3})O_3$ as labeled in Figure 4.5 (b). This indicated the chemical inhomogeneities and incomplete solid state reaction during sintering. It should be note that the intensity of second phase peaks was maximum at $x = 0.04$ and was decreased with increasing x. The appearance of Mg compound as second phase in the XRD pattern indicated the maximum solubility limit of BMN into BT lattice due to lowest diffusion rate determining step. Thus, the change in the phase

transformation of BT with addition can be attributed to the substitution of Mg or Nb on Ti-sites. Since the solubility of MgO in BT has been reported that was approximately with x = 0.02 [14, 22], the amount of the precipitated TiO_2 was expected to be x = 0.02; it will be too small amount to be detected by XRD. Therefore, in this study it was found that the maximum solubility limit was about x = 0.03 of BMN from P2 processing.

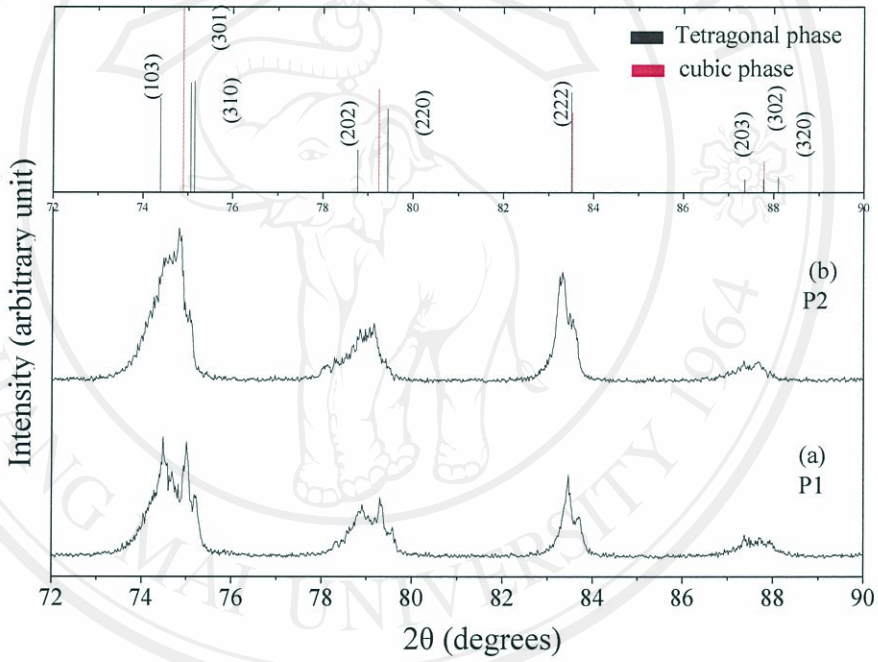

Figure 4.4 X-ray diffractions of ceramic samples with x = 0.02 showing tetragonal peak splitting at high angles by (a) P1 and (b) P2 processing.

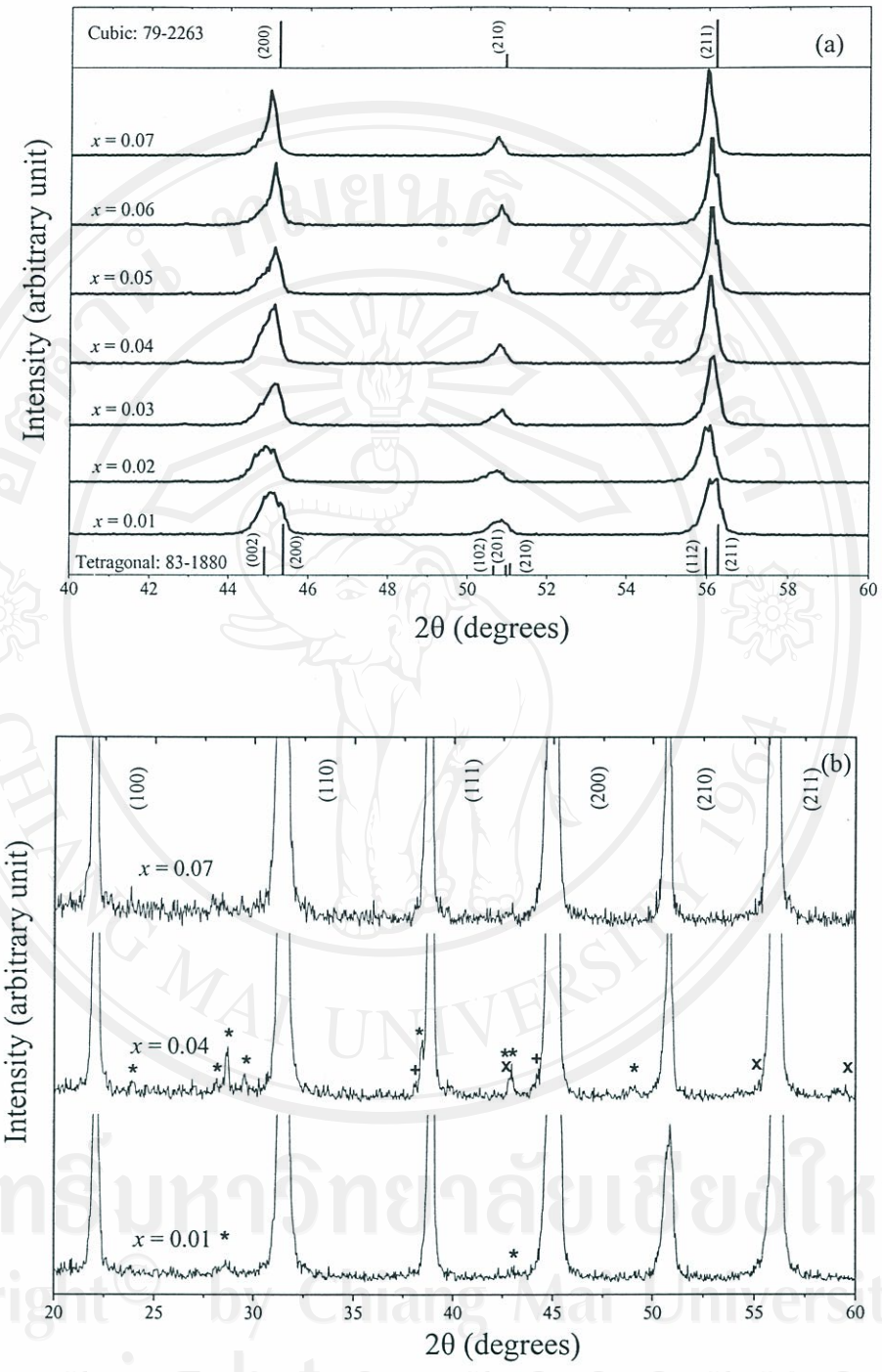

Figure 4.5 X-ray diffractions of samples sintered at 1400°C from P2 processing showing; (a) phase formation with as a function of x and (b) second phase formation; * indicating $Ba_6Ti_{17}O_{40}$, + : $Ba(Mg_{1/3}Nb_{2/3})O_3$ and x : $Ba_4MgTi_{11}O_{27}$.

Moreover, the effect of sintering temperature on the tetragonal splitting of at the angles 45°- 60° has been presented in Figure 4.6 (a), (b). From the Figure 4.6 (a), it had be seen that the tetragonal splitting of P1 sample was slightly decreased with increasing sintering temperature which exhibited the highest *c/a* value of about 1.0075. Tetragonal diminution phenomenon may be cause by high temperature promoted rise diffusion rate of additives into BT lattice which effected on lattice distortion. However, no significant of this effect on P2 samples was found. Figure 4.6 (b) showed the tiny splitting of the (200) and (002) peaks with highest sintering temperature, 1450 °C, showed the highest *c/a* value was about 1.0058. This indicating more high temperature was required to promote ferroelectric phase and to decrease the second phase in P2 processing preparation.

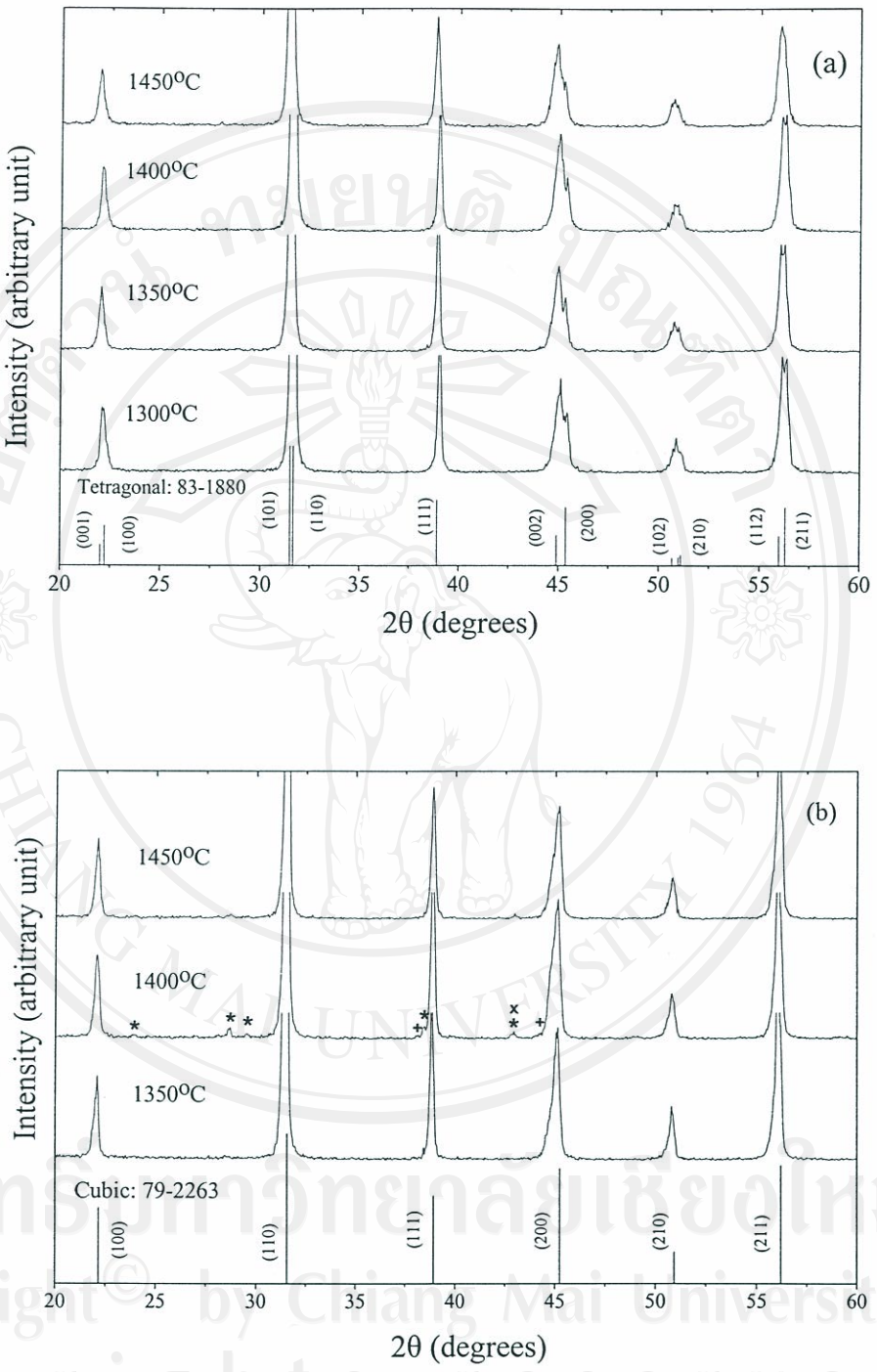

Figure 4.6 X-ray diffraction patterns of ceramics showing phase formation with various sintering temperatures; (a) $x = 0.02$ added samples from P1 processing and (b) $x = 0.04$ added samples from P2 processing. Second phase formation; * indicating $Ba_6Ti_{17}O_{40}$, + : $Ba(Mg_{1/3}Nb_{2/3})O_3$ and x : $Ba_4MgTi_{11}O_{27}$.

4.3 Lattice Parameters Estimation

The effect of additives on the lattice parameter was expected to be diminished the tetragonality [15, 22, 23, 34-36] cause by different of ionic radius. The solubility mode was monitored by the behavior of the lattice parameters as a function of x. A change in composition generally produces a change in lattice parameter and, therefore, a shift in the position of the diffraction peaks of that phase (A clear shift of the diffraction peaks to higher 2θ values with increasing x can be in Figure 4.3 (a), 4.5 (a)). The a lattice parameter increases if the solute Mg^{2+} has an atomic size larger than that of the solvent, Ti^{4+}. If the solid solution is non cubic (has unequal lattice parameters), the one of the parameters may increase and the other may decrease, but the unit-cell volume always increase. The reverse is true if the atomic size of the solute (Nb^{5+}) is smaller than that of the solvent (Ti^{4+}) [62]. In this study, the lattice parameter was calculate from splitting of (200) and (002) peaks at the angle 45° as shown in Figure 4.7 (a), (b). According to the data, the Mg^{2+} substitution is showed the effect of larger ionic radius more than that from Nb^{5+} on the lattice parameter. Samples from both processing, showed the c lattice parameter decreased with increasing amount of additives whereas the value of a lattice parameter increased slightly with x, which results in reduction in the tetragonality of Mg/Nb modified BT ceramics. This result is quite agreed with Brzozowski and Nagai [34, 22] who found the decreasing of tetragonality of BT phase with doped Mg^{2+} and Nb^{5+}, respectively. For $x = 0.05$, the value of c/a is nearly to 1, demonstrating that the average symmetry of the sample becomes cubic. It should be note that the slope of c/a graph of sample form P1 processing is sharper than P2, indicating clearer phase transformation. This result can be confirmed the cubic-tetragonal transformation from XRD results.

Moreover, this result indicated that the additive has diffused into BT lattice during sintering. In the cubic phase, *a* lattice parameter increased slightly with increasing *x*, indicated that unit-cell expansion.

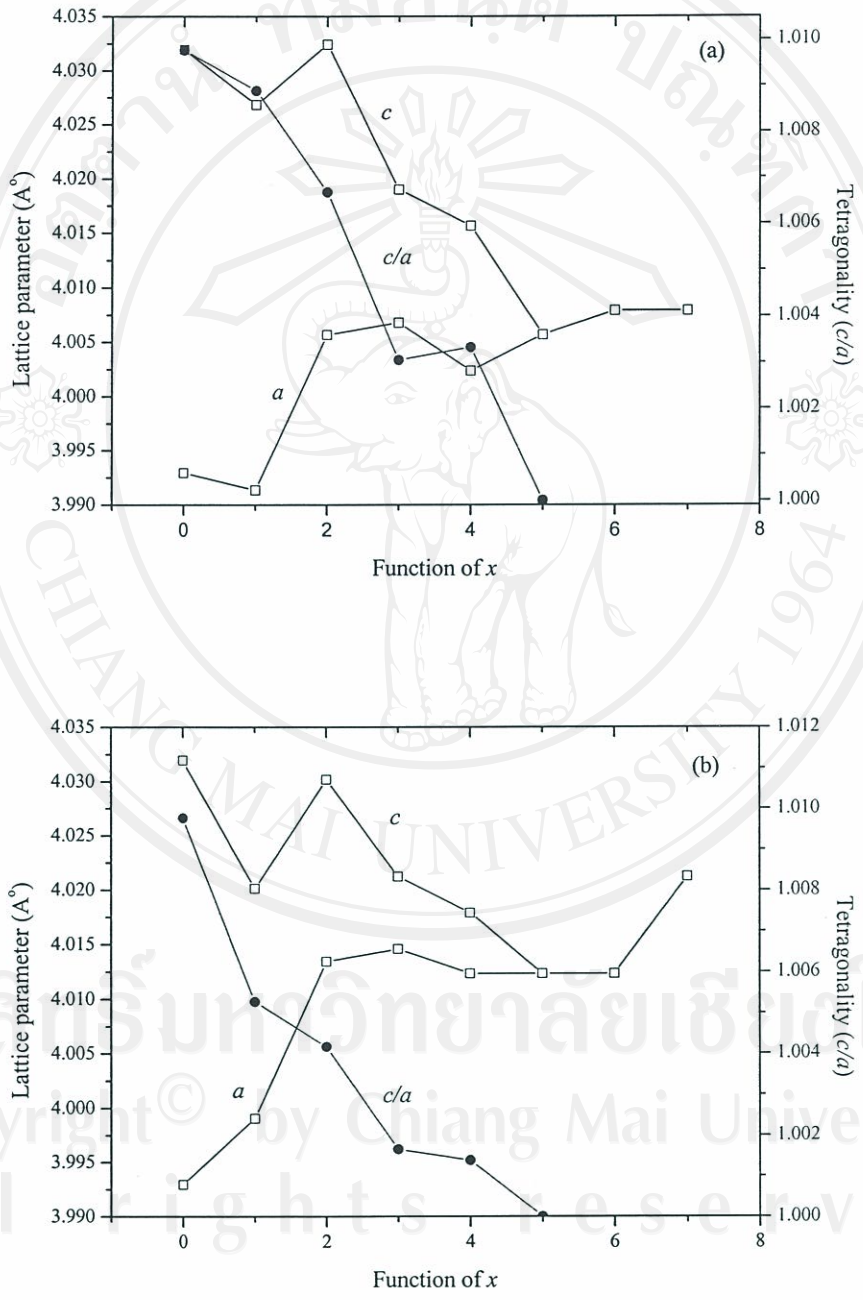

Figure 4.7 Lattice parameters of xBa($Mg_{1/3}Nb_{2/3}$)O_3 - (1-x)$BaTiO_3$ as a function of x ; (a) P1 processing and (b) P2 processing.

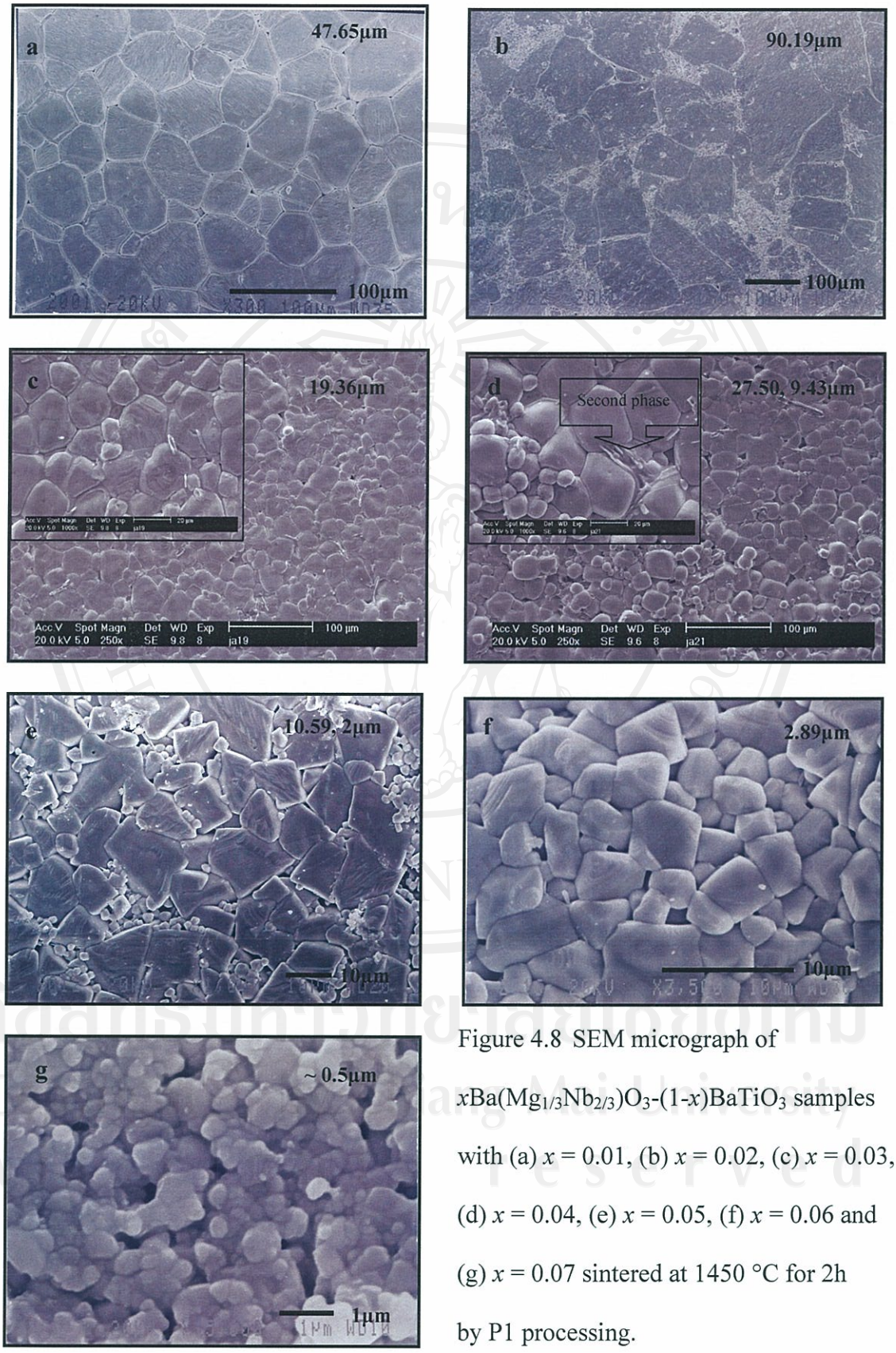

Figure 4.8 SEM micrograph of xBa($Mg_{1/3}Nb_{2/3}$)O_3-(1-x)$BaTiO_3$ samples with (a) x = 0.01, (b) x = 0.02, (c) x = 0.03, (d) x = 0.04, (e) x = 0.05, (f) x = 0.06 and (g) x = 0.07 sintered at 1450 °C for 2h by P1 processing.

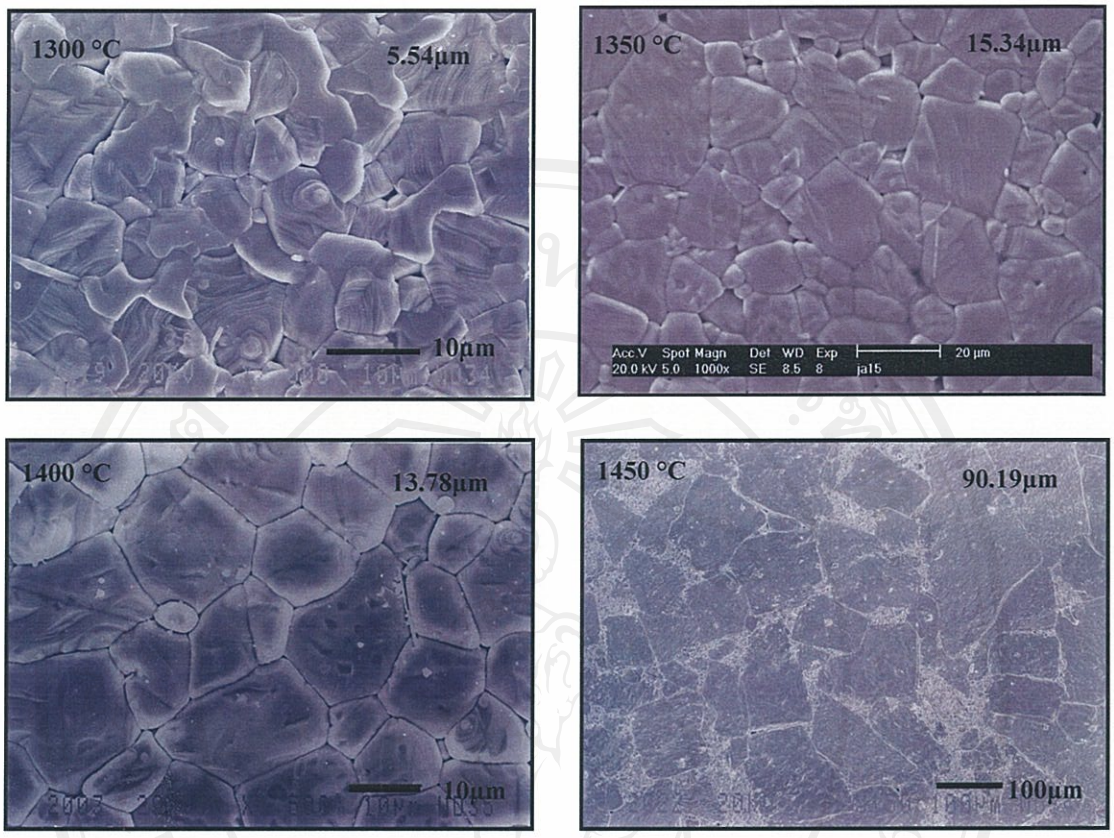

Figure 4.9 Shows the microstructure of $x = 0.02$ samples with prepared by P1 method, sintering at different temperature; 1300 °C, 1350 °C, 1400 °C and 1450 °C.

4.4 Microstructure Evolution of xBa($Mg_{1/3}Nb_{2/3}$)O_3-(1-x)$BaTiO_3$ Ceramics

To compare the effect of processing (P1 and P2) on microstructure. The microstructures were observed using scanning electron microscopy as shown in Figure 4.8-4.11. It was found that additives have a profound effect on the microstructural evolution of BT. According to literature has been reported that a major role of additives, $Nb^{5+}$and Mg^{2+} is their ability to influence the grain growth mechanism. The MgO/Nb_2O_5 additive's role in retarding the grain growth. It is well known that additives located at grain boundaries usually act as grain growth inhibitors [36, 63, 64]. Considering that in this study, the Mg^{2+} ions are not complete diffuse

into the BT lattice, remaining at the grain boundary due to lower solubility than Nb^{5+}ions. The XRD results obtained in this work confirm that expectation. The SEM images of P1 and P2 samples against composition x has been shown in Figure 4.8-4.10. From the pictures, it was found that within low concentration x = 0-0.03, the grain growth was significantly inhibit, average grain size was decreased. A bimodal grain size distribution is observed at x = 0.04-0.05 and uniform fine-grain microstructure was achieved with increasing x in both processes. The same result was found by Weill *et. al.* [49]. This phenomenon occurs in the system contains a non-homogeneous additives distribution the additive enriched regions present limited grain growth and high secondary phase precipitation at grain boundary. Conversely, the additive deficient regions showed exaggerated grain growth and strong intragrain porosity as can be seen in Figure 4.11. On the other hand, the development of a second phase with the appearance of elongated needles took place (Figure 4.8 (D) and 4.10 (C)). The XRD and EPMA analyses (as shown in 4.7) revealed that the second phase regions were $Ba_6Ti_{17}O_{40}$ and $Ba_4MgTi_{11}O_{27}$. This result is quite agreed with Yoon, Brzozowski and Rahaman [34, 35, 47] who found second phase, $Ba_6Ti_{17}O_{40}$ in Nb-doped BT system. The effect of sintering temperature on the microstructure was shown in Figure 4.9 and 4.11. The SEM images revealed that at low concentration x = 0.02 samples showed grain growth with increasing sintering temperature (Figure 4.9). This is because, phase correspond to Ti-excess region sample in BaO-TiO_2 phase diagram which showed liquid phase at grain boundary. At the critical concentration, x = 0.04 samples showed the significant grain growth inhibitor cause by second phase pinch at grain boundary. Moreover, the cracking was found inside the sample cause to reduce the density of the sample.

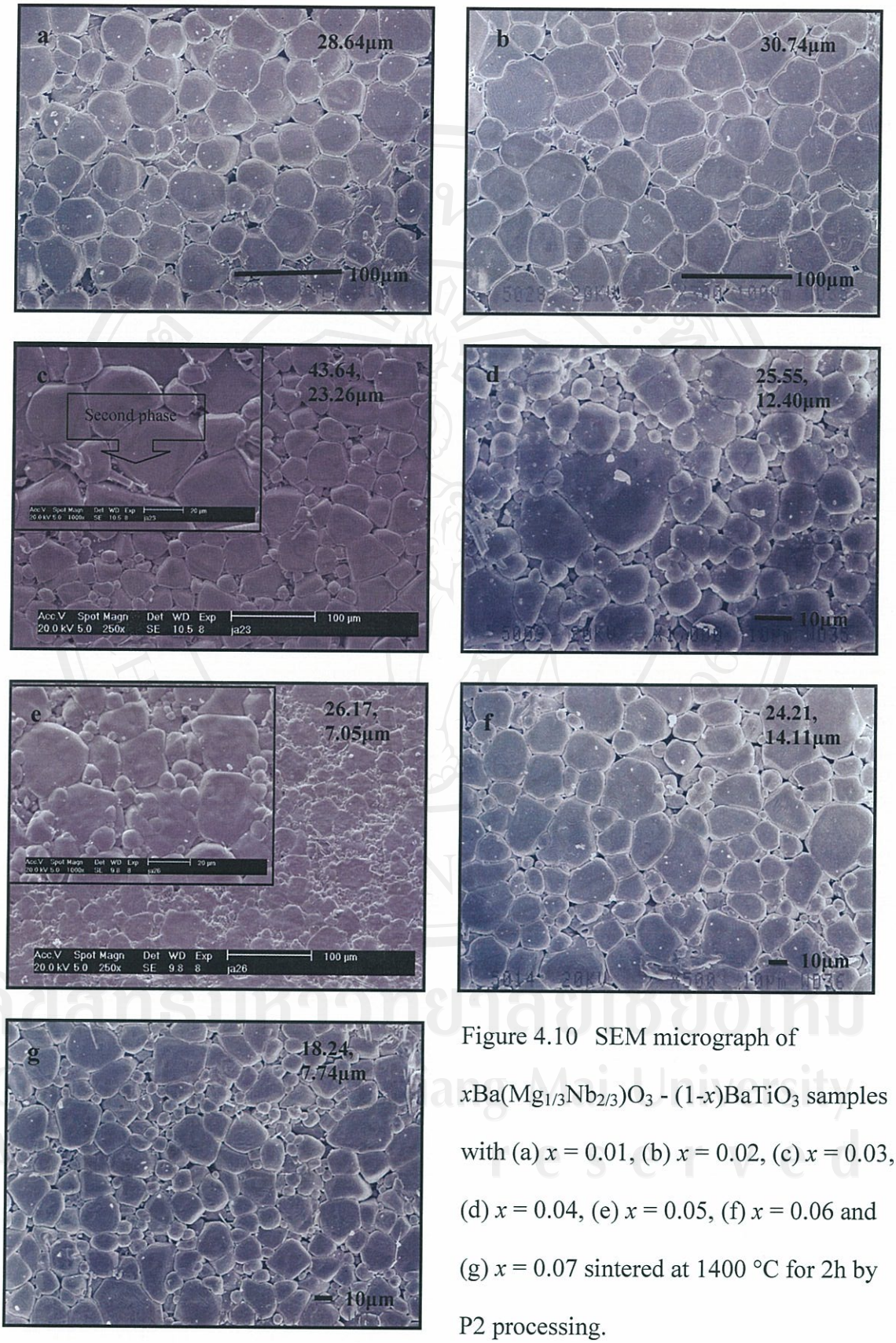

Figure 4.10 SEM micrograph of xBa($Mg_{1/3}Nb_{2/3}$)O_3 - (1-x)$BaTiO_3$ samples with (a) x = 0.01, (b) x = 0.02, (c) x = 0.03, (d) x = 0.04, (e) x = 0.05, (f) x = 0.06 and (g) x = 0.07 sintered at 1400 °C for 2h by P2 processing.

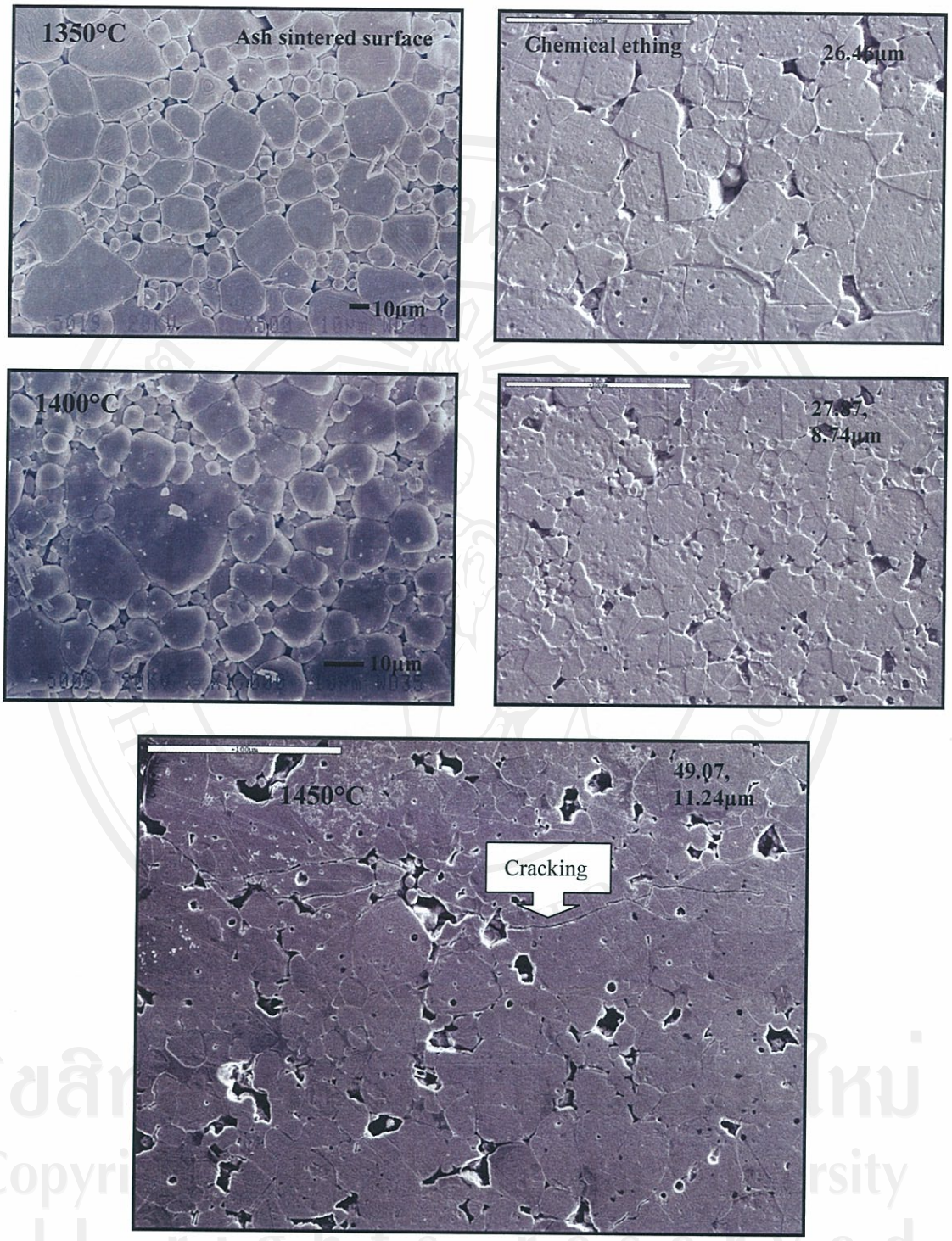

Figure 4.11 Shows the microstructure of $x = 0.04$ samples with prepared by P2 processing, sintering at different temperature; 1350 °C, 1400 °C and 1450 °C.

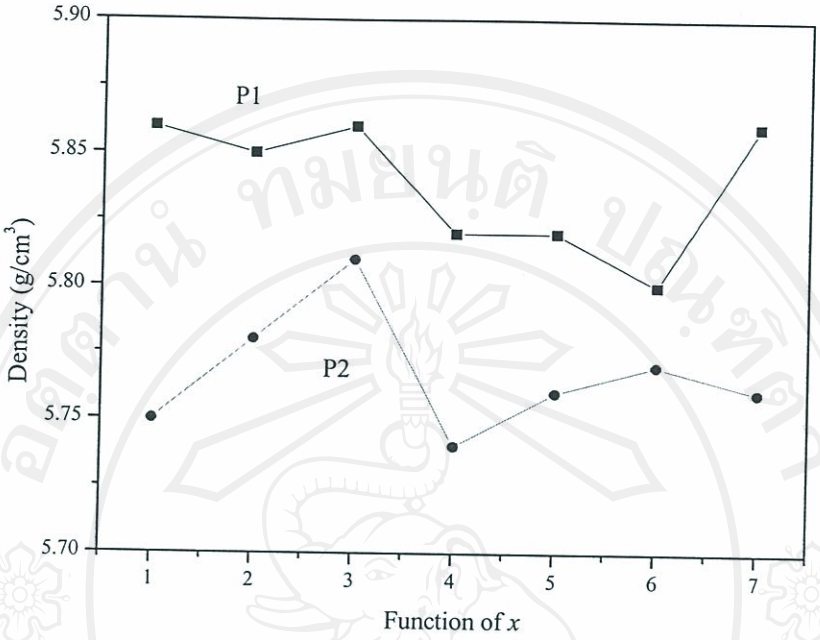

Figure 4.12 Density of sintered samples with P1 and P2 processing against different amount of x.

4.5 Densification Measurement

The sintering of BT is also depent on the stoichiometry of the compound. In this study, as most of additives Nb^{5+} and Mg^{2+} ions solubilise into the BT lattice at Ti-site, there is segregation of Titanium in the whole system. For BT materials with a small excess of TiO_2, the excess TiO_2 reacts with BT to form a second phase which becomes close to the composition $Ba_6Ti_{17}O_{40}$ (seen in Figure 4.3 and 4.5), which has a eutectic with BT at ≈ 1320 °C [8]. The liquid phase which form above the eutectic temperature is beneficial for densification. In our study, BT ceramic with a slightly Ti-excess composition were reported to have a higher sintered density. From the Figure 4.12, it was found that all of specimens showed the relative density above 95

and 93 percent of the theoretical density for samples from P1 and P2, respectively. It should be noted that the high sintering temperature was needed to promote densification with increasing the amount of additives. According the result, it can be seen that P1 samples showed the higher density than P2 in all of composition. At the low concentration of additives (x = 0.01-0.03) lead to abnormal grain growth along with intra and intergranular porosity (Figure is not shown). This phenomenon is responsible for decrease in the density values with respect to pure-BT. On the other hand, the decrease in density at increasing $x \geq 0.04$ may be due to the greater amounts of liquid being produced, from which an increasing amount of the lower density 6:17 phase, crystallized. The reported density of $Ba_6Ti_{17}O_{40}$ phase is 4.79 g/cm^3 compared to value of 6.02 g/cm^3 for BT calculated from the JCPDS file No. 79-2263. The highest density measured for the sample added with x = 0.03 is associated to more uniform grain microstructure that get in both P1 and P2 processing. However, the second phases presumable act as structural defects and generate microcrack, especially in the sample added with x = 0.04. This result can be confirmed by SEM micrograph in Figure 4.11. At x = 0.04 of P2 sample, showed the lowest density of the ceramic was slightly dropped (off 1.5 percent) due to exhibit discontinuous grain growth in the specimen and loosen the packing. After that the density values do not significant changes when increasing x above 0.04. This cracking reflected by a noticeable decrease in the tetragonality of BT as the nominal composition becomes higher in the additives which to reduce internal stress. It is not clearly why at x = 0.07 for P1 sample showed the good density. It may be cause by uniform and fine-grain packing.

TABLE 4.2 Physical properties of sintered ceramics with varied x and sintering temperature.

P1 Processing				P2 Processing		
Sintering Temperature (°C)	% Linear Shrinkage	Density (g/cm^3)	Function of x	Sintering Temperature (°C)	% Linear Shrinkage	Density (g/cm^3)
1350	13.71	5.84	0.01	1300	15.41	5.74
1400	13.47	5.84		1350	14.08	5.71
1450	13.65	5.86		1400	14.57	5.75
1300	15.81	5.85	0.02	1250	15.21	5.59
1350	15.72	5.81		1300	15.56	5.64
1400	15.93	5.80		1350	16.59	5.78
1450	15.80	5.80		1400	14.57	5.75
1400	15.60	5.80	0.03	1300	15.99	5.81
1450	15.46	5.84		1350	15.83	5.75
1500	15.50	5.86		1400	16.09	5.61
1400	15.95	5.61	0.04	1350	15.78	5.70
1450	15.90	5.76		1400	15.97	5.70
1500	15.77	5.82		1450	15.20	5.74
1400	15.68	5.81	0.05	1350	15.72	5.72
1450	15.62	5.82		1400	15.67	5.74
1500	15.23	5.70		1450	14.98	5.76
1400	16.27	5.80	0.06	1400	14.52	5.69
1450	16.90	5.76		1450	14.26	5.77
1500	16.29	5.78		1500	13.75	5.65
1450	16.32	5.77	0.07	1400	16.26	5.76
1500	16.17	5.86		1450	15.78	5.71
1550	15.18	5.79		1500	15.75	5.70

According to shrinkage data, in general, the shrinkage depends on the densification enhancement usually associated with grain growth, which occurs particularly when discontinuous grain growth begins. In this study, the linear shrinkage was about 13-16 percent for P1 and P2 samples. Physical properties of all composition can be shown in TABLE 4.2.

4.6 Phase Distribution by Back-scattered Electron Imaging (BEI), X-ray Mapping and Energy Dispersive X-ray (EDX)

The compositional differences within the microstructures were carried out by using back-scattered SEM imaging, along with X-ray mapping and EDX, which was preformed on polished sections of the sintered ceramics, as shown in Figure 4.13-4.14.

The back-scattering images in Figure 4.13 showed coexistence of two phases in bulk ceramic. The matrix phase is referred to as phase M and the second phase is referred to as phase S was found at grain boundary. From the images, it can be seen the grain boundary thickness of P1 and P2 samples was increased with increasing x. Moreover, it was found that P1 samples showed the S phase thickness at grain boundary narrower than that of P2 in the same doping concentration, indicated that S phase can occur easier by P2 processing. For $x = 0.07$ of P1 sample, S phase changes to elongated oval shape and can not find grain boundary.

The mapping technique was used to determine and confirm the Mg, Nb, Ba and Ti distribution region on bulk and grain boundary as shown in Figure. 4.14. At $x = 0.07$ was used to be demonstration of element distribution by this technique due to resolution limited of instrument. The M phase is from the strong scattering

heavy atoms (Ba and Nb), whereas the S phase at grain boundary are second phase from the weaker scattering element of Mg. However, Ti ions appeared in both bright and dark areas. To confirm these results the points at M phase and S phase on the P2 sample with x = 0.07 was performed to analyze the elemental gradient by EDX technique. The EDX data indicated that Nb^{5+} ions which were found only in M phase whereas Mg^{2+} ions were detected both in M and S phases. However, Mg^{2+} was rich at S phase. Considering at M phase, it was found that the percent of Ti element was slightly decreased with increasing x that indicating the substitution of additives were only occurred at Ti-site. However, the percent of Ba was not significant changed. Concerning at S phase, it was found that the percent of Ti element is nearly double of Ba concentration, indicated that the residual BMN can react with TiO_2-excess segregated at grain boundary to form the Mg-Ti-rich as S phase. These results showed Nb^{5+} ions diffused into the grain but Mg^{2+} ion can diffused into the grain only small portion most of them stayed at grain boundary. It was thought that the Mg^{2+} has low reactivity or inert to diffuse in BT. This was confirmed by EPMA technique, as shown in TABLE 4.3.

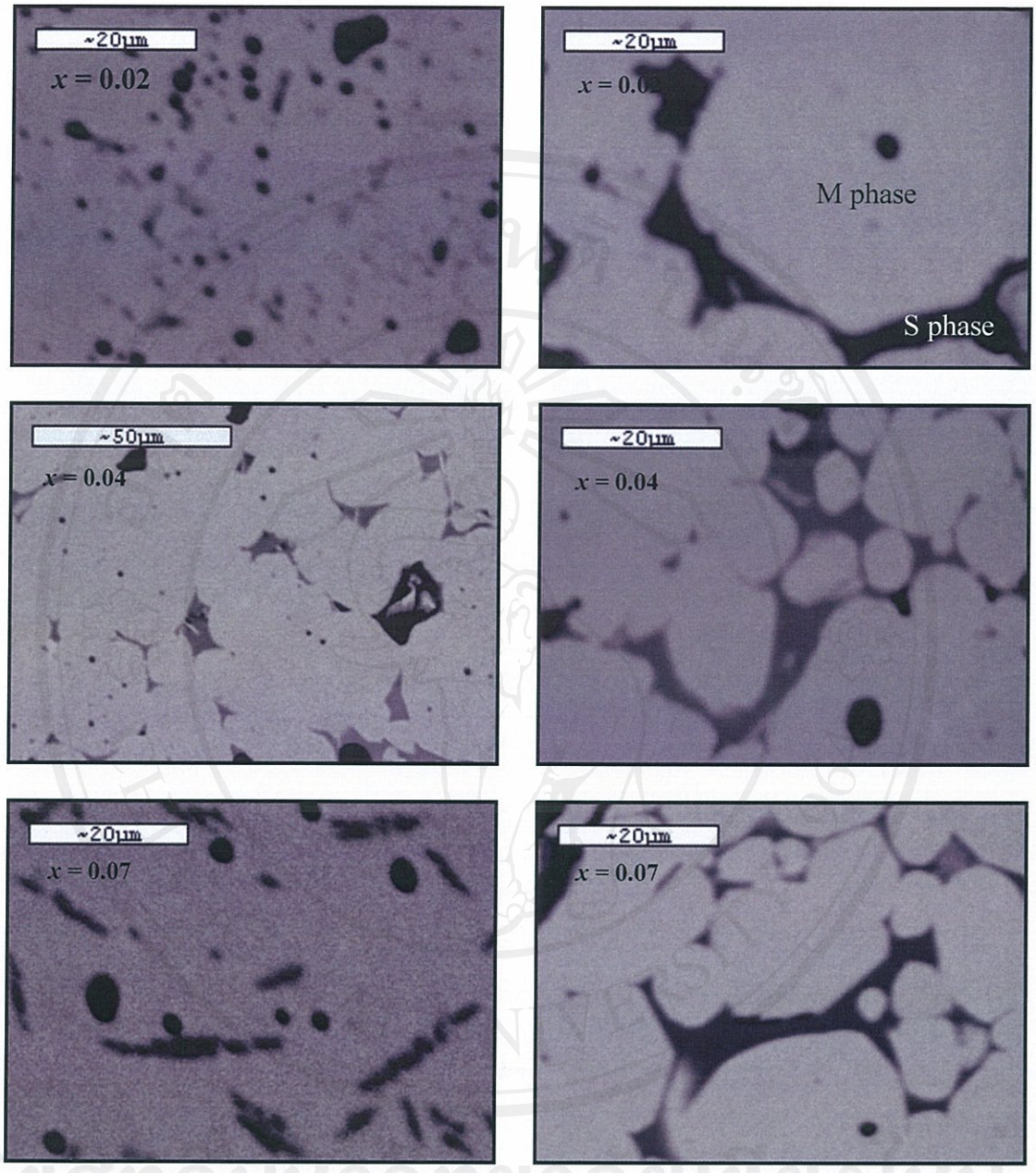

Figure 4.13 Back scattering micrographs of $x = 0.02$, 0.04 and 0.07 of additives ceramics prepared by (a) P1 and (b) P2 processing.

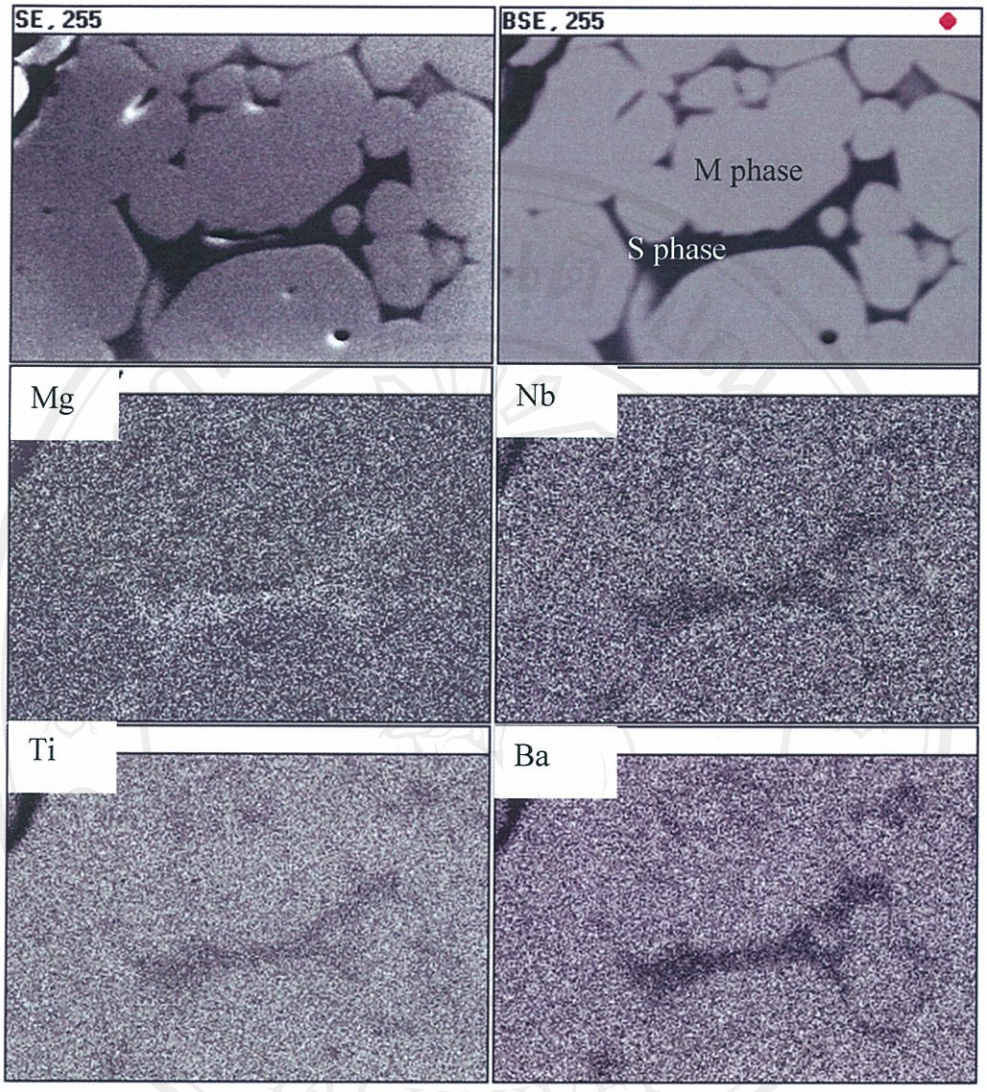

Figure 4.14 Micrographs mapping of samples with $x = 0.07$ of additives prepared by P2 processing. SE = SEM micrograph, BSE = Back scattering micrograph and the bottom 4 pictures are the X-ray mapping of Mg, Nb, Ti and Ba ions.

4.7 Quantitative Phase Analysis

An electron probe microanalysis (EPMA) was used to confirm the phase distribution on phase composition in microstructure. From the back scattering images (Figure 4.13) showed two phases in the polish surface as referred to M and S phases. The chemical composition analysis made by EPMA can provide the elemental concentration of Ba, Ti, Mg, Nb and O in the sample. Results from the EPMA quantitatives analysis of atomic percent which are average from 10 data points. Due to S phase of P1 sample with $x = 0.02$, the area was too small for EPMA technique. So, the analysis of the chemical composition was done for sample with $x = 0.04$ and 0.07 only as shown in TABLE 4.3.

Considering at M phase, all of results showed that percent of Ba is close to 20 (theory value as shown in TABLE 4.3), indicated that all additives occupied at Ti-sites only. The M phase composition of P2 samples was showed the percentage of elemental closer to the theory value than that from P1 samples. It is suggested that due to the different diffuse ability of additives as MgO, Nb_2O_5 and BMN into BT lattice. In case P1 sample, it can be seen that the percentage of Mg was lower than the theory value whereas the percentage of Nb was quite close to theory value. These results showed Nb^{5+} ions diffused into the grain whereas Mg^{2+} ions can diffused into the grain only small portion most of them stayed at grain boundary. It was thought that the MgO has low reactivity or inert to diffuse in BT and should be segregated at grain boundary. From this result, it can suggest that chemical concentration gradient of additives of P1 samples was occurred by this reason. However, the composition of M phase is good agreed with the calculated atomic percentage of nominal starting

composition ($0.04Ba(Mg_{1/3}Nb_{2/3})O_3$-$0.96BaTiO_3$ and $0.07Ba(Mg_{1/3}Nb_{2/3})O_3$-$0.93BaTiO_3$) in both processing.

Considering at S phase, for P1 samples with x = 0.04, the chemical composition showed low concentration of Mg and Nb (0.84 and 0.15 percent, respectively) which can ignore it. The Ba: Ti+Mg+Nb: O ratio is given approximately 9.7: 24.65: 62.68. Therefore, this phase suggests to be $Ba_6Ti_{17}O_{40}$. But in case of P2 sample at x = 0.04, it was found that S phase have two composition. First, with low concentration of Mg and Nb this should be match with $Ba_6Ti_{17}O_{40}$ as well. Second, with high concentration of Mg (about 3.85 percent) is close to the composition of $Ba_4MgTi_{11}O_{27}$. The same result was found at x = 0.07 for P2 sample. These result showed the coexistence of $Ba_4MgTi_{11}O_{27}$ and $Ba_6Ti_{17}O_{40}$ as second phase in P2 system whereas P1 system found only $Ba_6Ti_{17}O_{40}$.

TABLE 4.3 Average results of EPMA quantitative analysis of samples with varied x.

Composition x	Elemental (Atomic percent)				
	Ba	Ti	Mg	Nb	O
Theory atomic % of $Ba_6Ti_{17}O_{40}$	9.5	27	-	-	63.5
Theory atomic % $Ba_4MgTi_{11}O_{27}$	9.3	25.6	2.33	-	62.8
Theory atomic % $x = 0.04$	20	19.2	0.26	0.53	60
P1 at M phase	20.28±0.12	18.96±0.08	0.19±0.01	0.54±0.02	59.91±0.03
at S phase	9.71±0.12	23.66±0.17	0.84±0.24	0.15±0.03	62.68±0.06
P2 at M phase	20.16±0.13	18.57±0.12	0.19±0.02	0.44±0.05	59.92±0.05
at S phase	9.58±0.15	25.12±0.5	1.95±0.06	0.06±0.02	62.68±0.28
	9.56	24.25	3.85	0.03	62.18
Theory atomic % $x = 0.07$	20	18.6	0.462	0.933	60
P1 at M phase	20.08±0.05	18.59±0.13	0.30±0.02	0.71±0.03	59.92±0.01
at S phase	Can not point out because area is not suitable				
P2 at M phase	20.18±0.28	18.62±0.28	0.38±0.10	0.86±0.06	59.95±0.10
at S phase	10.30±0.02	25.51±0.06	0.58±0.69	0.26±0.01	62.95±0.04
	9.99±0.17	24.11±0.02	3.67±0.15	0.09±0.02	62.12±0.02

4.8 Dielectric Behaviour of xBa($Mg_{1/3}Nb_{2/3}$)O_3-(1-x)$BaTiO_3$ Ceramics by P1 Processing

Barium titanate (BT) is known as a typical ferroelectric material which exhibits sharp transition obeys first-order ferroelectric-paraelectric phase transition [8, 10, 18-21]. BT based solid solutions with partial substitution of the Ti-site position by other cation to get smeared out in dielectric constant around the Curie temperature (T_c), i.e. to exhibit diffuse phase transition (DPT), a similar behavior to well known complex ferroelectric relaxor.

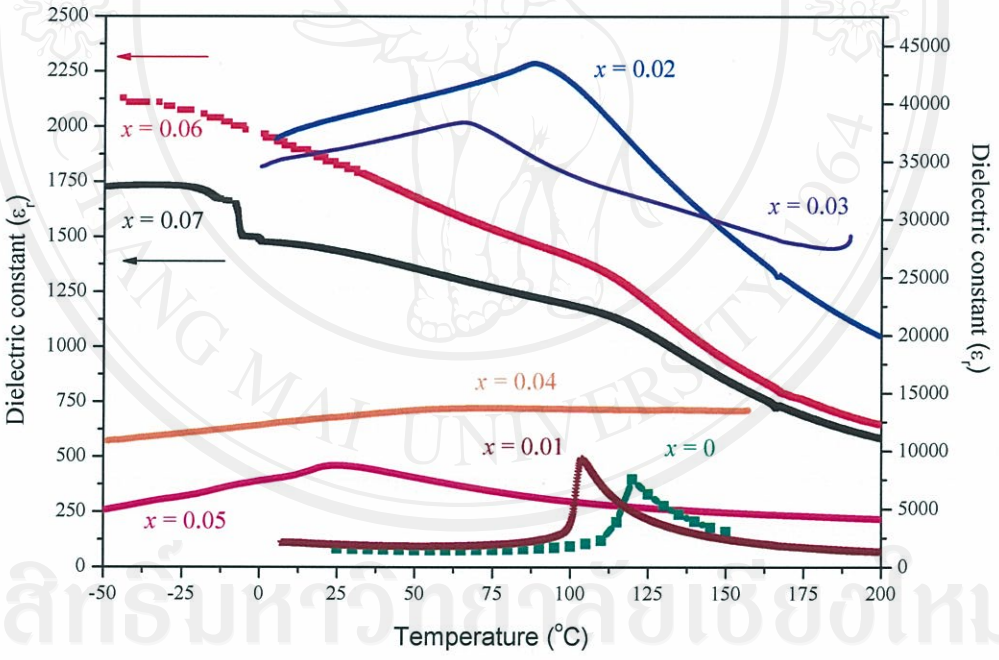

Figure 4.15 Temperature variation of dielectric constant ε_r of the xBa($Mg_{1/3}Nb_{2/3}$)O_3 -(1-x)$BaTiO_3$ ceramics, x = 0-0.07 at 1 kHz with prepared by P1 processing.
(x = 0-0.05 show dielectric constant value in the right hand axis and
x = 0.06-0.07 show dielectric constant value in the left hand axis)

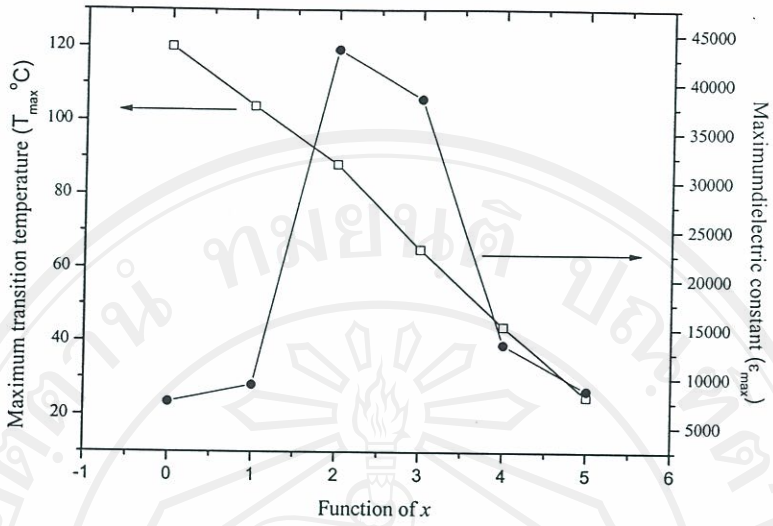

Figure 4.16 Maximum dielectric constant and transition temperature versus function of x with prepared by P1 processing.

Substitution of Ti-site by Magnesium ion (Mg^{2+}) as acceptor coexist Niobium ion (Nb^{5+}) as donor, the enlarge of dielectric constant around T_c for ceramic specimen was reported by Weill *et al.* [48,49] with used chemical route preparation.

In this study, substitution of Ti-site by Magnesium ion (Mg^{2+}) as acceptor coexist Niobium ion (Nb^{5+}) as donor was prepared by solid solution mixed oxides method. The characteristic temperature of the dielectric constant of xBa($Mg_{1/3}Nb_{2/3}$)O_3-(1-x)$BaTiO_3$, x = 0-0.07, is shown in Figure 4.15. From these data, the maximum dielectric constant increased from 1,600 to 40,000 in the composition range $0 \leq x \leq 0.02$, then decreased with increasing x. This is due to reduce the tetragonality and increase the impurity of second phase in ceramics with $x \geq 0.03$ of BMN that can see in Figure 4.7(a). This result is agreed with Brzozowski and Nagai [22, 34] who found the decreasing of the tetragonality of BT phase with

doped Nb^{5+} and Mg^{2+}, respectively. Moreover, from these plots were found to be broadened with increasing fraction of x. The maximum dielectric constant ε_{max} and T_c as a function of the fraction of x are presented in Figure 4.16. A clear transition in T_c decreased continuously with increased of x. There is a good linear relationship between T_c and x, indicating that this system is a well behaved solid solution. The broadened peaks of xBa($Mg_{1/3}Nb_{2/3}$)O_3-(1-x)$BaTiO_3$, $x \geq 0.02$ indicated that the phase transition are of diffused type. The broadness of the peak is an indicative of the disorder that exists on Ti-site position to make the nano-region of inhomogeneous composition in the specimens. When Ti^{4+} (0.75Å) in the B-site is substituted by larger Mg^{2+} (0.86Å) ion, the occupation needed more space, which gives rise to decreasing the rattling space for the cations at the center of oxygen octahedra. Conversely, Ti-site is substituted by smaller Nb^{5+} (0.69Å) ion, the smaller space are needed, which gives rise to increase the ionic displacements. This would result in mixing the various displacements of cations in the specimen to exhibit comprises regions with different local Curie point and respond with different temperature. The net effect is the diffuse phase transition was exhibited. The same result realized by Prasad [65].

The present work reports the dielectric properties of Mg/Nb-substituted BT ceramic solid solutions in whole range of x = 0-0.05. In order to investigate its influence on the dielectric properties of solid solution on an attempt to examine the possible effect of inhomogeneities on DPT behavior. The degree of broadening or diffuseness (δ_γ) in the observed dielectric variation could be estimated with the diffusivity (γ) using the expression [66]

$$\varepsilon_{max}/\varepsilon = 1 + \frac{(T - Tm)^{\gamma}}{2\delta_{\gamma}^{2}} \quad (1 \le \gamma \le 2) \text{ or}$$

$$\log\left(\varepsilon_{max}/\varepsilon - 1\right) = \gamma \log(T - Tm) - \log\left(1/2\delta_{\gamma}^{2}\right) \qquad (4.1)$$

The value of γ was found to be 1 for a sharp ferroelectric-paraelectric phase transition (i.e. obeying Curie-Weiss law), and γ = 2 for completely disorder ferroelectric system having a diffuse phase transition in ceramics. The corresponding their properties were listed in TABLE 4.4. The value of γ vary between 1.12-1.80, which confirmed that diffuse phase transitions occur in xBa($Mg_{1/3}Nb_{2/3}$)O_3-(1-x)$BaTiO_3$ ceramics due to higher degree of disorder at Ti-site position. In addition, the parameter δ_γ can be used to measure the degree of diffuseness of phase transition. The mean value of δ_γ is extracted from these plots by fitting a linear equation that can be shown in Figure 4.17. The δ_γ values of composition in the xBa($Mg_{1/3}Nb_{2/3}$)O_3-(1-x)$BaTiO_3$ system are listed in TABLE 4.4 showed the δ_γ tend to increase with an increased in fraction of additives with x = 0.01–0.04. At x = 0.04 composition showed the maximum diffuseness of phase transition value about 133 and decreased these value with x = 0.05 of additives that showed the maximum solubility limit in this system [64]. However, the values of δ_γ and γ are both material constants depending on the composition and structure of the material.

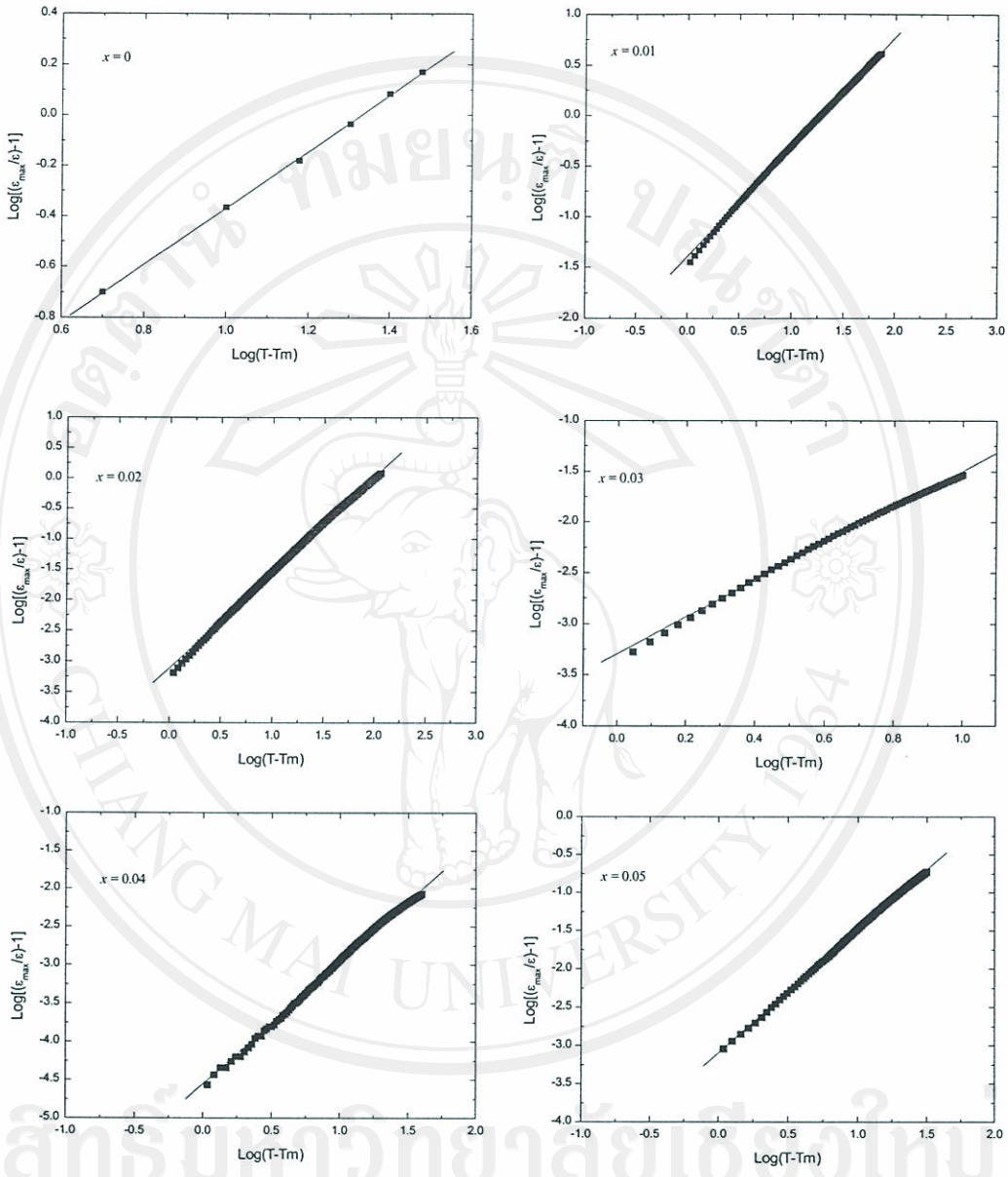

Figure 4.17 Log [($\varepsilon_{max}/\varepsilon$)-1] vs Log (T-Tm) for xBa($Mg_{1/3}Nb_{2/3}$)O_3-(1-x)$BaTiO_3$ ceramics, x = 0-0.05 with prepared by P1 processing.

Figure 4.18 showed the temperature dependence of the loss tangent (tanδ) at 1 kHz. It was observed that, for the composition with $x = 0$, tanδ had a very low value and remained constant about 0.005. For the added specimens, tanδ slightly increased at room temperature, for $x = 0.03$ of additives presented the maximum value of tanδ of about 0.1 compared with $x = 0$ specimen. And tended to increased with increasing the temperature, especially at $x = 0.02$ sample showed the highest tanδ value was 0.3 at high temperature over T_c. It may be due to thermal activated space charge conduction which can happen with dielectric and semiconductor at high temperature. The obtained result is in agreement with Yoon and Das [45, 67] that found this effect on their material. On the other hand, which is caused by the influence of leakage conductivity that was produced by the chemistry defect reaction shows that

As donor, $$Nb_2O_5 + 2Ti_{Ti} \rightarrow 2Nb_{Ti}^{\bullet} + \tfrac{1}{2}O_2 + 2e' + 2TiO_2$$

As acceptor, $$MgO + Ti_{Ti} + O_O \rightarrow Mg_{Ti}'' + V_O^{\bullet\bullet} + TiO_2$$

However, at $x \geq 0.05$ samples, it changes into an insulator again because of the formation of ionic defects which compensate for the extracharge from additives. On the other hand, it is assumed that the insulating region is built due to additives segregation phenomenon due to influence of defect and the impurities are accumulated at the grain boundary, leading to and enhancing the insulating region. In addition to it, additives segregation and vacancies formation pin grain boundary mobility during sintering, inhibiting grain growth which can not present the semiconducting effect on fine grain.

Moreover, highly additives BT ceramics are yellow in color, indicated that exhibit an extremely high resistivity ($\approx 10^{10}$ Ω.cm) at room temperature as shown in TABLE 4.4.

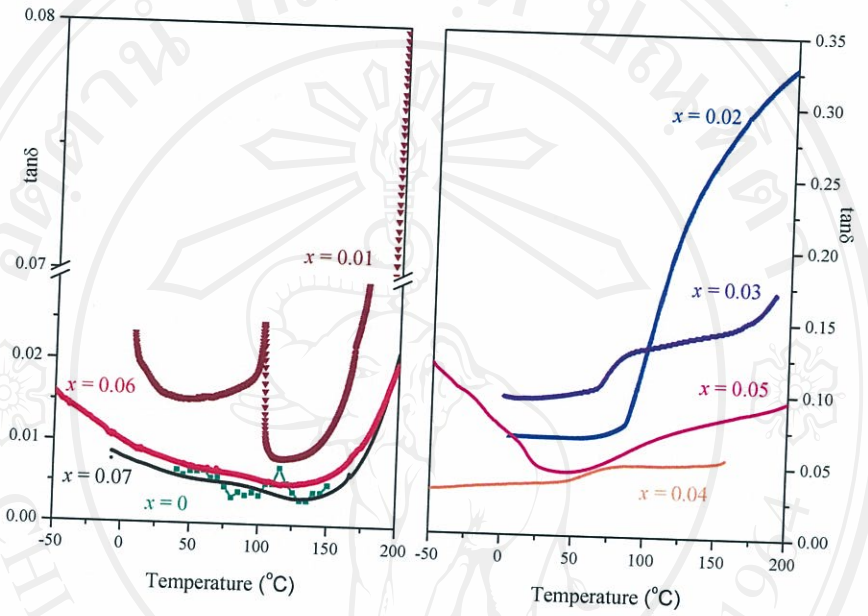

Figure 4.18 Temperature variation of tanδ of the xBa($Mg_{1/3}Nb_{2/3}$)O_3-(1-x)$BaTiO_3$ ceramics, x = 0-0.07 mole at 1kHz with prepared by P1 processing.

TABLE 4.4 Dielectric properties of xBa($Mg_{1/3}Nb_{2/3}$)O_3-(1-x)$BaTiO_3$ by P1 processing.

Composition of x	T_{max} (°C)	ε_{max} at 1 kHz	tanδ at T_{max}	ε_r at 25°C	tanδ at 25°C	γ	δ_γ	ρ(Ω.cm)	Avg grain size (μm)
0 (1300°C)	120	7,558	0.005	1,600	0.006	1.12	3.92	$\approx 10^{13}$	≈ 100
0.01(1450°C)	109.5	8,176	0.008	1,890	0.016	1.09	3.52	2.6×10^{10}	47.65
0.02 (1300°C)	88	43,000	0.085	38,787	0.068	1.57	25.38	7.9×10^{7}	5.54
0.03(1450°C)	65.5	38,400	0.103	36,086	0.096	1.80	31.27	2.8×10^{6}	19.36
0.04(1450°C)	54	13,673	0.041	12,906	0.036	1.60	133.84	2.4×10^{6}	16.31
0.05(1450°C)	24.5	8,737	0.049	8,737	0.048	1.60	24.90	5.8×10^{8}	10.59
0.06(1450°C)	-	1825	0.008	1800	0.008	-	-	2.4×10^{10}	2.89
0.07(1450°C)	-	1434	0.007	1400	0.007	-	-	2.6×10^{10}	~0.5

4.9 Dielectric Behaviour of xBa($Mg_{1/3}Nb_{2/3}$)O_3-(1-x)$BaTiO_3$ Ceramics by P2 Processing

In this case, BMN-substituted BT ceramic in whole range of x = 0-0.07 were prepared by mixing BT and BMN via mixed oxides method. The combination of BMN (x) into BT is expected to be the broaden peak of dielectric constant with indicated the DPT and shifted the T_c downward. The dielectric plots obtained in this work confirm that expectation. In general, T_c, dielectric constant and spontaneous polarization are largely dependent on the ionic displacement associated with the sample. The difference of x in the samples showed variation of displacement to produce the DPT in this system. The dielectric constant-temperature characteristics of sintered samples are shown in Figure 4.19. From the graph, it was found that BMN have a profound influence on the dielectric constant and DPT. The role of BMN is their ability to smear out of dielectric constant peak. From the data, the maximum dielectric constant increased from 7,500 to 13,000 at T_c (~ 102 °C) in the composition range $0 \leq x \leq 0.02$, then decreased within the composition range $0.03 \leq x \leq 0.04$. After that at x = 0.05, sample showed the maximum dielectric constant was about 13,300 at 18 °C. The T_c decreases accompanied by peak broadening, with increasing x. The maximum dielectric constant and T_c as a function of fraction of BMN (x) are presented in Figure 4.20. The T_c decreases continuously with increase in x. This suggests that there is no significant change in the crystal structure of BT with BMN concentration. The broadness, δ_γ and diffusivity, γ are estimated by plots of Log $[(\varepsilon_{max}/\varepsilon)-1]$ versus Log (T-Tm) were generated for $0 \leq x \leq 0.05$, as shown in Figure 4.21. The mean value of δ_γ and γ are calculated from equation 4.1 as can be shown in TABLE 4.5.

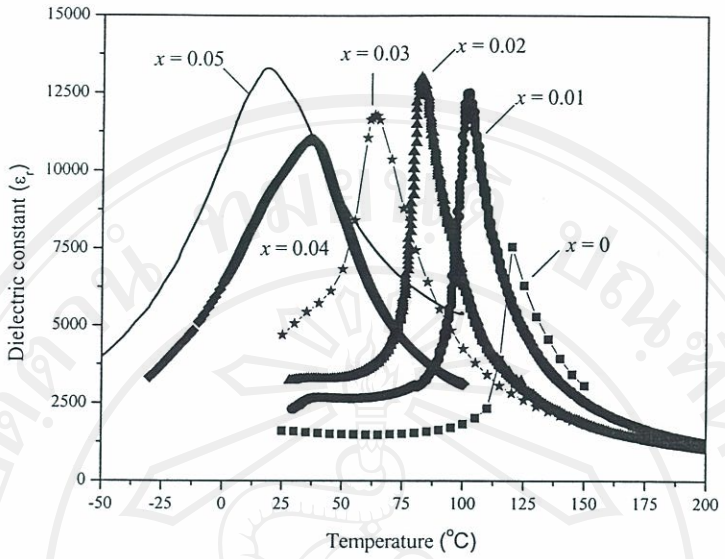

Figure 4.19 Temperature variation of dielectric constant ε_r of the xBa($Mg_{1/3}Nb_{2/3}$)O_3 -(1-x)$BaTiO_3$ ceramics, x = 0-0.05 at 1 kHz with prepared by P2 processing.

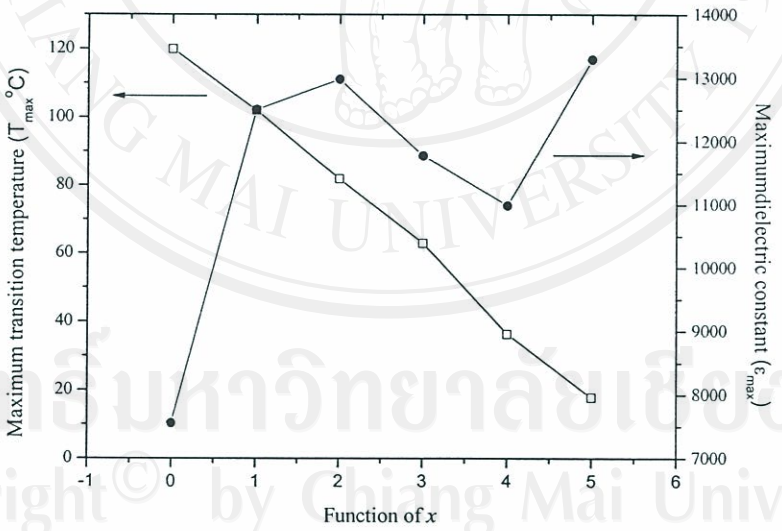

Figure 4.20 Maximum dielectric constant and transition temperature versus function of x with prepared by P2 processing.

The broadness, δ_γ of the peak is to some extent is an indicative of the disorder that exists on certain sites apart from the contributions arising out of inhomogeneties. From the TABLE 4.5, it is found that degree of diffuseness, γ increase from 1.12-1.62 in the composition range $0 \leq x \leq 0.04$, the decreased with $x = 0.05$. Moreover, the δ_γ value is increased with increasing x of about 3.61-15.55.

It should be note that the ceramic from P1 process showed flatter characteristic and high value of dielectric than with ceramic from P2 processing which compared at same composition. It may be cause by the individual oxides of MgO and Nb_2O_5 are easier diffuse than compound BMN to produce concentration gradient in the sample. This reason is confirmed by diffuseness (δ_γ) and diffusivity (γ) value in TABLE 4.4-4.5. On the other hand, P2 samples have a lot of contamination with second phase and low density due to reduce the dielectric constant.

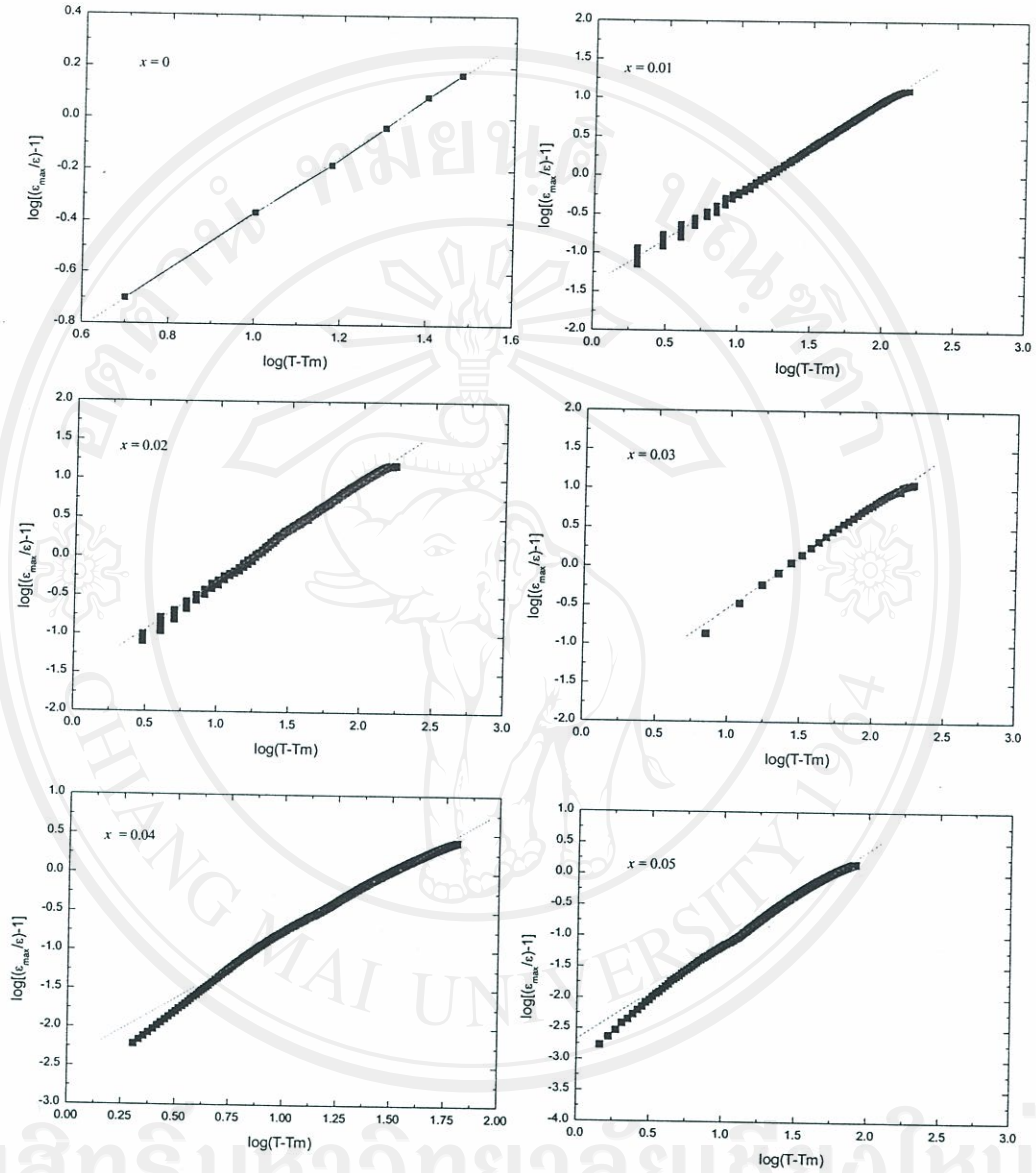

Figure 4.21 Log $[(\varepsilon_{max}/\varepsilon)-1]$ vs Log (T-Tm) for xBa($Mg_{1/3}Nb_{2/3}$)O_3-(1-x)$BaTiO_3$ ceramics, x = 0-0.05 with prepared by P2 processing.

As can be seen from Figure 4.22, when temperature is higher than 150 °C, the curve of temperature dependence of tanδ warped upwards markedly with composition range $0 \leq x \leq 0.03$. Considering the possible defects in BT, $Nb_{Ti}^{\bullet}$, Mg_{Ti}'', V_{Ba}'', V_{Ti}''' and $\ddot{V}_O$ was occurred in the system. It may be cause by the influence of leakage conductivity. On the other hand, the rapid increase of tanδ at high temperatures in the low frequency region (i.e. 1 and 10 kHz) may be due to space charge polarization. At the high temperature, impurity ions in the bulk crystal matrices capture the surface electron, causing the space charge polarization at the surface. Unlikely, the sample with x = 0.04-0.05, it was found that the showed the high value of tanδ at low temperature was about 0.65 and 0.2, respectively. This result is reflected the semiconducting effect on high adding of BMN which reduce the resistivity of sample at room temperature.

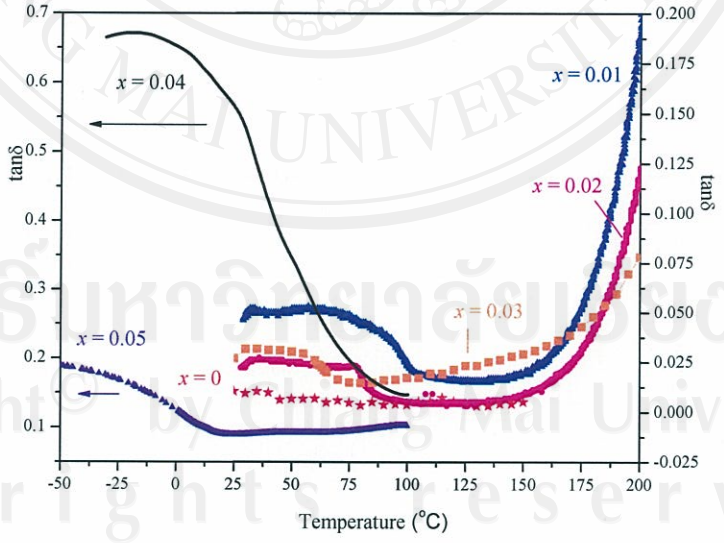

Figure 4.22 Temperature variation of loss tangent tanδ of the xBa($Mg_{1/3}Nb_{2/3}$)O_3 -(1-x)$BaTiO_3$ ceramics, x = 0-0.05 at 1kHz with prepared by P2 processing.

TABLE 4.5 Dielectric properties of xBa($Mg_{1/3}Nb_{2/3}$)O_3-(1-x)$BaTiO_3$ by P2 processing.

Composition of x	T_{max} (°C)	ε_{max} at 1 kHz	tanδ at T_{max}	ε_r at 25°C	tanδ at 25°C	γ	δ_γ	ρ(Ω.cm)	Avg grain size (μm)
0(1300°C)	120	7,558	0.005	1,600	0.006	1.12	3.92	$\approx 10^{13}$	~100
0.01(1400°C)	102	12,500	0.022	2,334	0.260	1.193	3.61	1.4×10^{10}	28.64
0.02(1400°C)	82	12,300	0.015	3,163	0.187	1.278	4.33	1.3×10^{10}	30.74
0.03(1400°C)	63	11,780	0.022	4,718	0.201	1.312	5.88	1.7×10^{10}	33.45
0.04(1350°C)	36.4	10,990	0.461	9,975	0.561	1.617	11.61	1.7×10^{7}	18.9
0.05(1400°C)	17.9	13,300	0.092	12,650	0.091	1.534	15.55	4.4×10^{7}	16.61
0.06(1400°C)	-	12,000	0.049	-	-	-	-	6.3×10^{9}	19.16
0.07(1400°C)	-	8,470	0.036	-	-	-	-	1.2×10^{10}	12.99